RESEARCH TOWARDS THE DESIGN OF A NOVEL SMART FLUID DAMPER USING A MCKIBBEN ACTUATOR

by

Haithem Ismail Elderrat
Submitted for the degree of Master of Philosophy

June 2013

The University Of Sheffield.

Department of Mechanical Engineering

Supervisors Dr Neil Sims and Dr Jem Rongong

SUMMARY

Vibration reducing performance of many mechanical systems, decreasing the quality of manufactured products, producing noise, generating fatigue in mechanical components, and producing an uncomfortable environment for human bodies. Vibration control is categorized as: active, passive, or semi-active, based on the power consumption of the control system and feedback or feed forward based on whether sensing is used to control vibration.

Semi-active vibration control is the most attractive method; one method of semi-active vibration control could be designed by using smart fluid. Smart fluids are able to modify their effective viscosity in response to an external stimulus such as a magnetic field. This unique characteristic can be utilised to build semi-active dampers for a wide variety of vibration control systems. Previous work has studied the application of smart fluids in semi-active dampers, where the kinetic energy of a vibrating structure can be dissipated in a controllable fashion.

A McKibben actuator is a device that consists of a rubber tube surrounded by braided fibre material. It has different advantages over a piston/cylinder actuator such as: a high power to weight ratio, low weight and less cost. Recently McKibben actuator has appeared in some semi-active vibration control devise. This report investigates the possibility of designing a Magnetorheological MR damper that seeks to reduce the friction in the device by integrating it with a McKibben actuator. In this thesis the concept of both smart fluid and McKibben actuator have been reviewed in depth, and methods of modelling and previous applications of devices made using these materials are also presented. The experimental part of the research includes: designing and modelling a McKibben actuator (using water) under static loads, and validating the model experimentally. The research ends by presenting conclusions and future work.

ACKNOWLEDGEMENTS

First of all I would like to thank Almighty Allah, whose blessings made it possible for me to carry out this work.

I would like to thank my supervisors: Dr Neil Sims and Dr Jem Rongong for their guidance and support throughout this project. I would also like to thank everyone in the department who have aided this research, particularly to Mr Mahmet Ali and Mr Leslie Morton for their assistance me during my study.

I would like to thank Libyan government for supporting my tuition and fees during this research study.

Last but not the least; I would like to give thanks for the support of my family and friends for their support and faith in me during the hardship.

TABLE OF CONTENTS

LIST OF FIGURES

NOMENCLATURE

Nomenclature	Meaning	Unit
A	Effective hydraulic area.	m
b	Length of uncoiled fiber.	m
c	Viscous damping	$N.s/m$
c_c	Critical damping.	$N.s/m$
$D_{\theta=90}$	Diameter of tube when θ=90 .	m
D_0	Unstrained diameter of McKibben tube.	m
D	Instantaneous diameter McKibben tube.	m
F	Force.	N
F_C	Column friction force	N
F_{ce}	Contractile force of McKibben tube.	N
F_v	Viscous friction force	N
F_f	Friction force	N
F_{max}	Maximum force of McKibben tube.	N
H	Applied magnetic field to smart fluid	A/m
I_1	Strain invariants.	$-$
k	Linearization actuator stiffness.	N/m
K_{fiber}	Stiffness of fiber material.	N/m
k	Stiffness constant of spring.	N/m
L	Instantaneous length of McKibben tube.	m
L_0	Unstrained length of McKibben tube.	m
dL	Axial displacement.	m
$L_{\max}$	Maximum length of McKibben tube.	m
$L_{\min}$	Minimum length of McKibben tube.	m
M	Mass	Kg
n	Number of turns.	$-$
P'	Gage pressure.	$N\ /m^2$
Q	Coulomb damping constant of McKibben actuator.	m
$\mathrm{t_k}$	Thickness of McKibben tube.	m
$\mathrm{t_0}$	Thickness of inner tube.	m

v	Actuator velocity at the top of McKibben tube.	$m\ /sec$
dV	Volume change of McKibben tube.	m^3
V	Volume of a McKibben tube.	m^3
$\mathrm{V_r}$	Volume is occupied by the inner tube.	m^3
W_{in}	Input work.	$N.m$
W_{out}	Output work.	$N.m$
W	Strain energy density function	N/m^2
ε	Strain	$-$
θ	Fiber's angle.	Degree
μ_r	Shear modulus of rubber.	$N\ /m^2$
μ	Viscosity of fluid	$N.s\ /m^2$
τ	Shear stress in smart fluid	$N\ /m^2$
τ_y	Yield shear stress in smart fluid	$N\ /m^2$
ζ	damping ratio	$-$
ω_n	Natural frequency	rad/s
$\dot{\gamma}$	Shear strain rate	sec^{-1}
$\lambda_i (i = 1,2,3)$	Principal stretches.	$-$

CHAPTER 1: INTRODUCTION

1-1 Vibration Control

Vibrations have bad effects on the performance of many structures and applications. Generally, there are three main approaches used to control vibrations; passive vibration control, active vibration control and semi-active vibration control. A passive system comprises springs and dampers which are the most traditional elements used to avoid unwanted vibrations. These elements are attached to the total mass of the system to form a suspension system. This suspension system reacts passively in opposition to the deflection caused by vibrations, and this movement causes the vibrations to be minimized. Due to its inherent simplicity and reliability, passive approaches are used in many varieties of engineering systems [1]. However, their performance is limited and constrained for structures that experience a wide variety of excitation conditions.

The second technique is active vibration control. In this method, an actuator and sensors are used instead of damping elements to react against unwanted vibration. This technique can usually achieve a high performance for eliminating vibration, and it has been used in different fields, such as: industrial applications [2], and in the field of transportation [3]. However, complexities in design, high cost and energy consumption are great disadvantages of active vibration control.

The third method is a semi-active vibration control; this has been developed to take advantage of the best features of both passive and active control systems. It is used to cope with the high cost and to maintain the optimum performance for an active vibration method. This can be achieved by operating semi-active dampers to produce force when there is necessity for vibration suppression, and switching off this force when energy input is required [4]. Semi active control can also be achieved by using elements that have adjustable parameters; smart materials and structures are used widely in this field. Smart material has the ability to modify its properties in response to vibrations and excitations, therefore it is able to provide excellent vibration control [5]. Examples of smart materials include: Shape Memory Alloy (SMA), piezoelectric material and smart fluid. McKibben actuators, which are utilized in human interaction devices in many applications [6], have been used in semi active vibration control as a variable damping structure [7].

Smart fluids are one example of smart materials, and are considered as the one of most superior means of controlling vibration [8], and lots of semi-active applications have been employed successfully. However, the majority of conventional smart fluid dampers have been designed by using a hydraulic actuator, which has a dry seal friction. This friction can have a negative effect on the vibration performance of the system.

To reduce the friction in the device, our aim is to use a McKibben actuator instead of a hydraulic actuator. This report investigates the possibility of designing a Magnetorheological MR damper by using a McKibben actuator instead of piston and cylinder actuator. This actuator has advantages over cylinder and piston dampers such as: high power/weight ratio and low cost. Although it has been used to into many applications in human interaction devices since the 1950s, it was recently noticed that this material has a variable damping structure. Therefore, it has appeared in some semi-active vibration control applications [7]. This research is to investigate the possibility of designing a novel smart fluid damper that seeks to reduce the friction in a device by integrating McKibben actuator. Therefore, the concept of smart fluid and McKibben actuator will now be presented in more detail.

1-2 Smart Fluid

Smart fluid is a fluid that changes its properties in response to an applied electric or magnetic field. It consists of micron sized particles suspended in an inert carrier liquid. There are two types of smart fluid; Electrorheological fluid (ER) and Magnetorheological fluid (MR). In ER fluid, the carrier liquid is dielectric and particles are semiconductors for electricity, while magnetisable particles dispersed in a non-magnetisable carrier liquid are used for MR fluids.

The flow behaviour of smart fluid is like a Newtonian fluid, where the relationship between the shear stress and shear strain rate of the fluid is linear. By applying an electric/magnetic field to the smart fluid, the behaviour of the fluid will be more similar to Bingham plastic fluid behaviour as shown in Figure 1-1. To interpret this modification microscopically, the particles are spread within the smart fluid without an electric/magnetic field; by applying an appropriate field, the particles are aligned into chains. Once aligned in this manner, the state of the fluid will change from a free-flowing liquid state to a solid-like state, and the behaviour of the fluid will be more like Bingham plastic fluid.

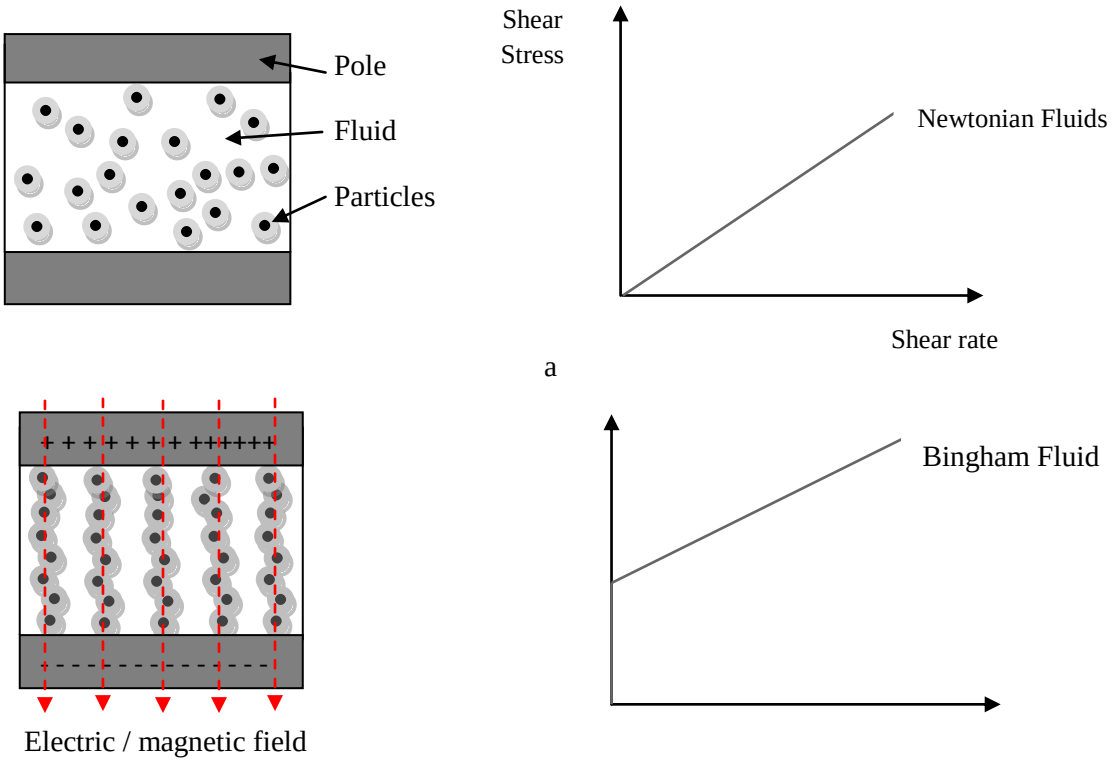

Figure 1-1 Smart fluid. (a) Characterizing of smart fluid without applying an external field, (b) characterizing of smart fluid by applying an external field.

As a result of applying an electric or magnetic field, a yield stress develops in the fluid. Smart fluid is capable of developing yield stress in only a few milliseconds. This yield is a function of an applied field, and increasing an applied field will lead to increasing the yield stress. Figure 1-2 show the change of yield stress and apparent viscosity by changing the applied field. The shear stress in smart fluid τ can be calculated by using the next expression.

$$\tau = \tau_y(H)sgn(\dot{\gamma}) + \mu\dot{\gamma} \qquad 1\text{-}1$$

Where: τ_y is the yielding shear stress controlled by the applied field H, μ is viscosity of fluid without applied magnetic field, $\dot{\gamma}$ is the shear strain rate, and sgn(·) is the signum function. Basically, there are three elements in a smart fluid: carrier fluid, suspended particles and stabilizing additives. For further details, a physical composition and operating mechanism have been demonstrated by Sims 1999 [9]. MR was a significant commercial success before ER fluid, due to advantages such as: MR fluid is capable of generating much higher yield stress; it is not sensitive to contaminants and it is less affected by variations of temperature [10]. Consequently, this research will focus on Magnetorheological Fluid.

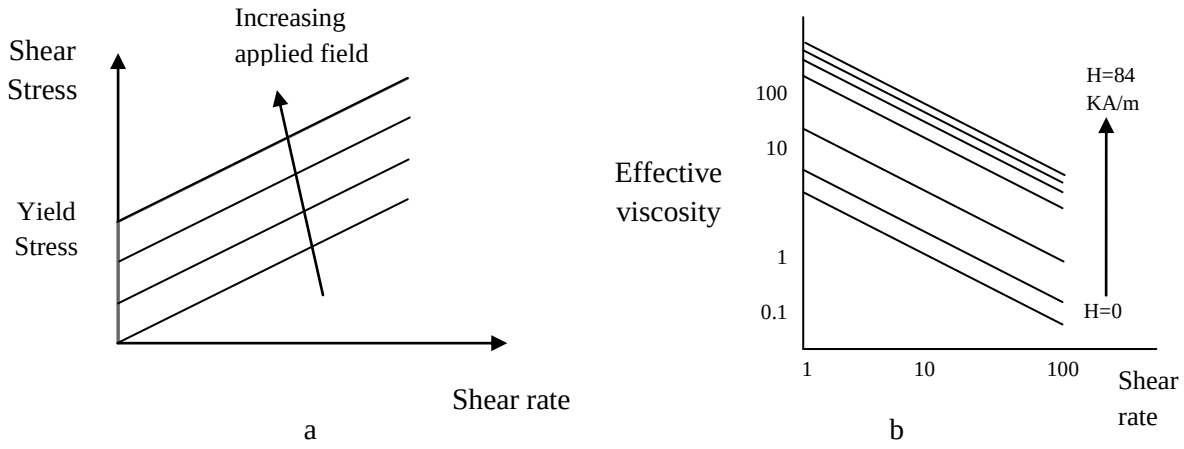

Figure 1-2 Variation of the shear stress and apparent viscosity with shear strain for an MR fluid under different magnetic field strengths: (a) Shear stress(b) the apparent viscosity [11].

1-3 Motivation for this study

The majority of smart fluid dampers are designed with normal hydraulic actuators that use a cylinder, piston and valve housed in the cylinder. The kinetic energy of a vibrating structure can be dissipated in a controllable manner by applying an electric/magnetic field to the valve. There are two kinds of friction used in the damping phenomenon which appear in a hydraulic actuator: Coulomb friction and viscous friction [12]. Coulomb friction represents friction associated with mechanical surfaces contacting together such as bearing friction, and friction in hinges. This friction is a constant and does not depend on the velocity of the body. Viscous friction represents the force required to push fluid through restrictive passages that may exist in the actuator such as orifices and valves, and it depends on the velocity of the body. The total actuator friction is the sum of Coulomb and viscous friction. Figure 1-3 shows these types of friction.

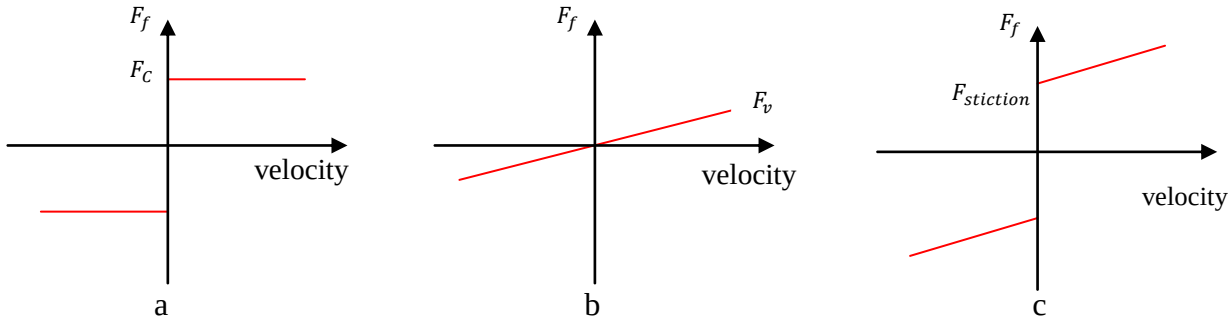

Figure 1-3 Friction in actuator: (a) Coulomb frictionF_C, (b) Viscous frictionF_v, (c) Total frictionF_F.

Although the friction has a positive effect in the damping devices, the dry sealing friction makes a vibration transmission to the equipment; this tiny vibration may cause poor accuracy for sensitive devices [13]. Friction could have a bad effect on the system when applied force is close to overcoming the static friction. The behaviour is called stick-slip motion. Stick-slip motion occurs at close to zero velocity and is in the form of a sudden jerking motion. Typically, the static friction coefficient between two surfaces is larger than the kinetic friction coefficient. If an applied force is large enough to overcome the static friction, the friction reduces from static to dynamic friction. The reduction of the friction can cause a sudden jump in the velocity of the movement. The system of two degree freedom will be taken as an example to illustrate this effect.

- **Two-degree-of-freedom System: 2DOF System**

Two degree of freedom systems are systems that require two independent coordinates to describe their motion; an example of this system is shown in Figure 1-4. The solution of these equations could be described by either time domain or frequency domain. In time domain, it is possible to plot time and amplitude of displacement or velocity or acceleration, while in frequency domain the relationship between frequency and amplitude can be plotted.

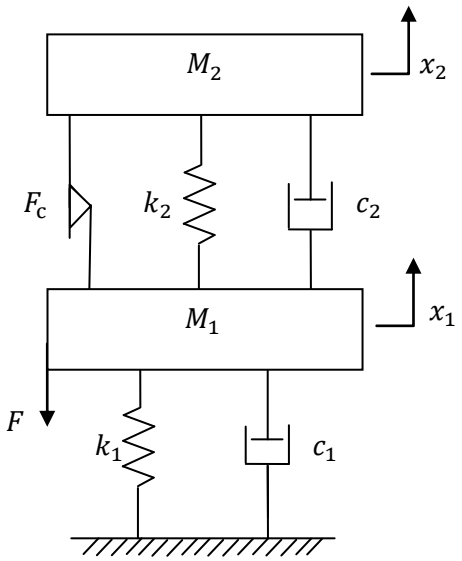

Figure 1-4 system of two degree of freedom.

By assuming the parameters of the system as displayed in Table 1-1, the Coulomb friction between masses has a value $F_c = 5N$, and applying force F=30N with varied frequency from 0.1 to 16 rad/s. The response of a structure is often characterised by its Frequency Response Function (FRF). Frequency Response Function (FRF) shows the amplitude of response at different frequencies for unit amplitude forcing. Figure 1-5 shows the magnification factor

motion. It is calculated by using $\frac{XK}{F}$. The stiffness of K_1 and force F are inputs of the system as shown in Table 1-1, while the value of amplitude of dynamic deflection X_1 was determined by using Matlab Simulink. The Frequency Response Function (FRF) in Figure 1-5 is achieved by using the Matlab Simulink and Matlab code as presented in Appendix A. The Figure shows; the amplitude of magnification factor has a low value at 4rad/s, while its maximum value is at 11rad/s. It also shows a smooth motion of the mass M_1, which is because applied force has overcome the Coulomb friction.

Table 1-1: Value of parameters

Parameters	Value
M_1	$50Kg$
M_2	$275Kg$
c_1	$80N.s/m$
c_2	$800\ N.s/m$
k_1	$230000\ N/m$
k_2	$30000\ N/m$
F	$30N$

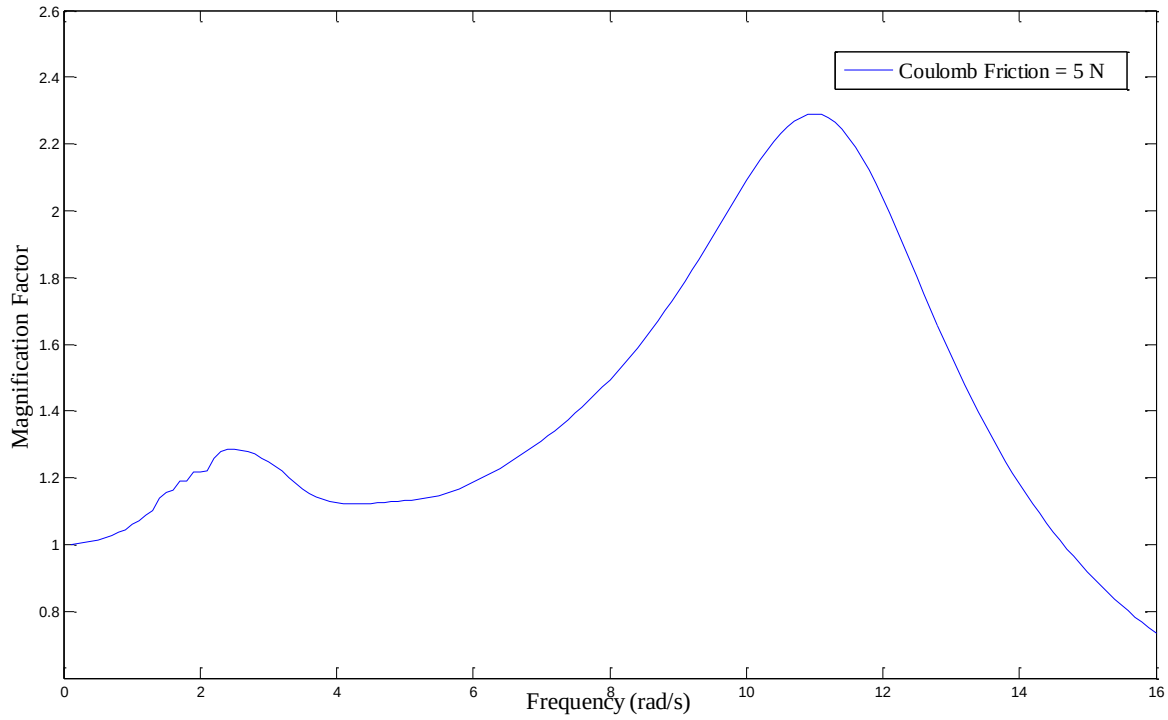

Figure 1-5 magnification factor FRF of mass M_1.

However, in the case where Coulomb friction has a high value, a tendency will exist for the motion to be intermittent rather than smooth. The two masses M_1 and M_2 will stick to each other and act as one mass. This will lead to an increase of the vibrations. Figure 1-4 shows the frequency response function (FRF) of the system at different values of Coulomb friction. The Figure shows that there is a jerk motion when Coulomb friction has a high value.

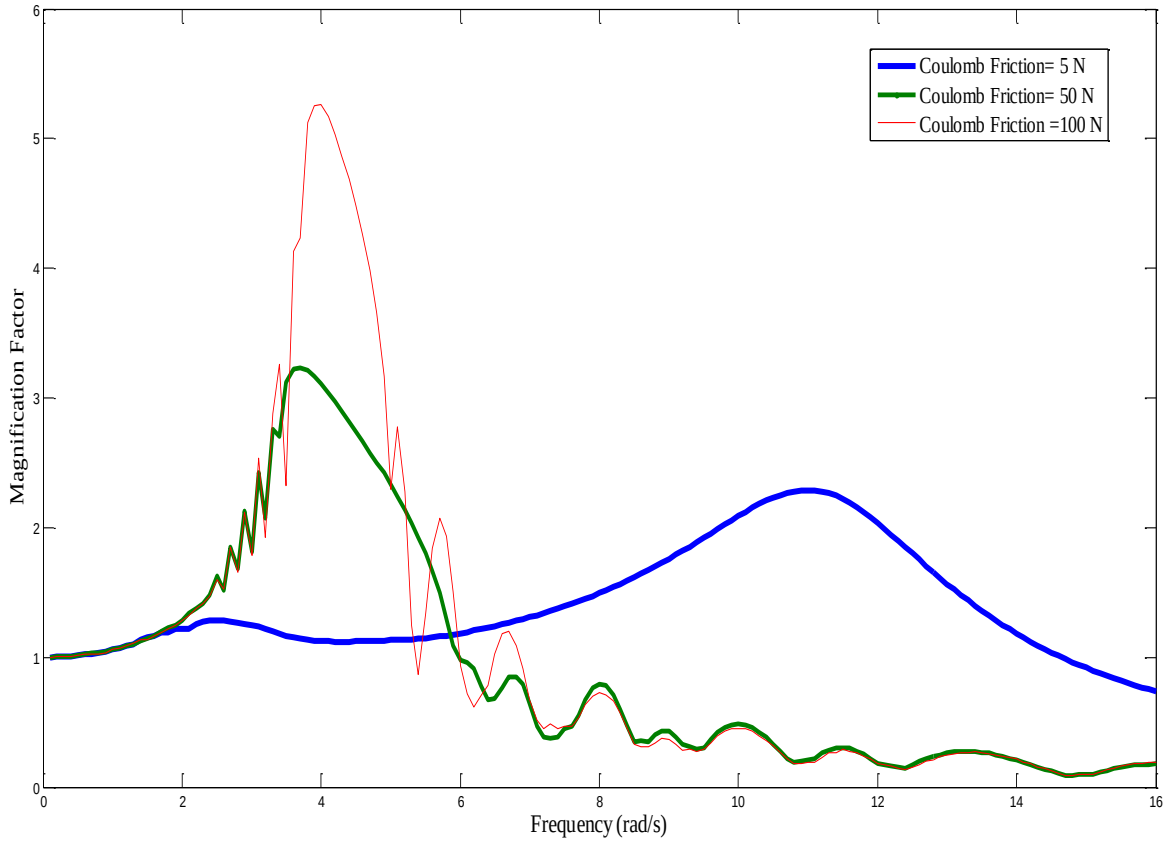

Figure 1-6 Magnification factor FRF of mass M_1 under different value of Coulomb friction.

Stick-slip friction is present to some degree in almost all actuators and mechanisms and is often responsible for performance limitations [14].

To overcome this issue, a McKibben actuator has a low value of static friction; so it is less affected by stick-slip phenomena. The next section will present the concept of the McKibben actuator.

1-4 McKibben Actuators

The McKibben actuator is a device that converts fluid pressure to force; it consists of an internal rubber tube inside a braided mesh shell. When the inner tube is inflated, the internal volume of the actuator will increase causing the actuator to expand axially as shown in Figure 1-7. These actuators were introduced in the 1950s. The McKibben actuator is usually used to mimic the behaviour of skeletal muscle [6]. It is also used in other applications for instance: robots [15], medical equipment [16] and industrial applications [17].

Although the working fluid in a McKibben actuator is usually air, there are some applications using water as a working fluid, especially in exoskeleton devices and devices working in a water medium, such as an actuator for an underwater robot introduced by Kenneth et al.[18]. Shan et al. developed a variable stiffness adaptive structure based upon fluidic flexible matrix composites (F^2MC) and water as the working fluid [19]. The fibres in an F^2MC actuator can be placed at any one angle or combination of angles. This material can be designed to bend and it also provides a greater axial force.

The advantages of the McKibben structure tubes are that it uses inexpensive and readily available materials, and it can easily be integrated into a structure. A McKibben actuator also offers others advantages such as being light weight and with low maintenance costs when compared to traditional cylinder actuators. A comparison of the force output of a pneumatic McKibben actuator and a pneumatic cylinder was made, and the result shows that the McKibben actuator produces a higher ratio of power to weight than the pneumatic cylinder actuator [20].

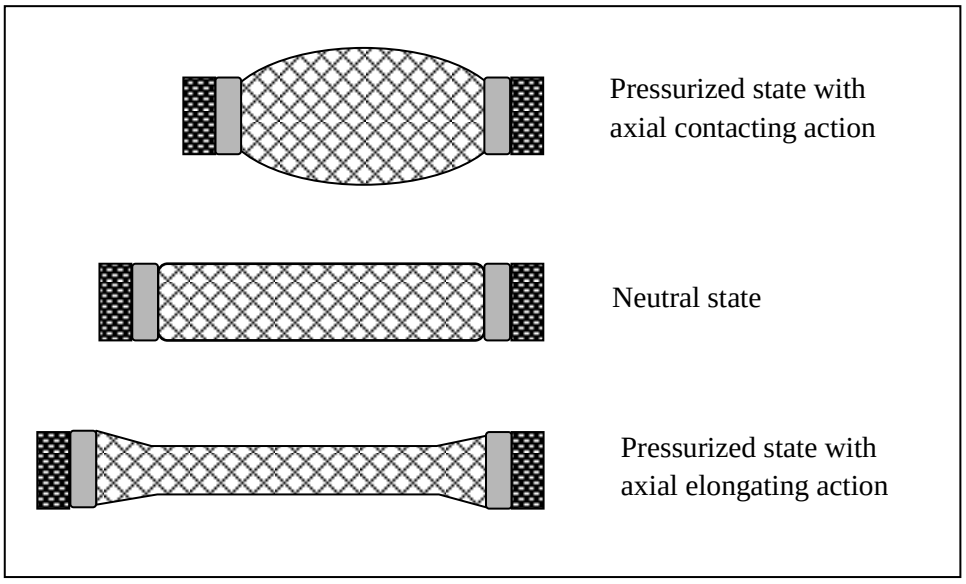

Figure 1-7: Concept of McKibben actuator.

In summary, two types of working fluids appeared in previous applications of McKibben actuators: air in McKibben muscles (i.e. a pneumatic actuator), and water in F^2MC applications and in some applications of artificial muscles. The present study is investigating the possibility of using a magneto-rheological fluid as a new working fluid in a McKibben actuator, and the capability of using a new application in controlling structural vibration.

1-5 Objectives and Organization of the Research

The motivation of this project is to investigate a novel design of smart fluid damper that seeks to reduce the friction in a device. This thesis is the first step toward accomplishing this mission, therefore the aim of this project is to study the possibility of designing a low friction Magnetorheological (MR) damper using the McKibben actuator concept. To achieve this aim the following objectives should be achieved.

- Investigate and understand the principles of smart fluids, especially concerning their modelling control.
- Investigate and understand the principles of flexible composite material and the McKibben actuator.
- Reproduce the basic modelling approaches of a McKibben actuator.
- Design and commission a rig of fluidic flexible matrix composite materials, and model and validate the system under static load.

1-6 Structure of the Research

This research consists of five chapters which are organized as follows:

Chapter 1: This chapter provides the different methods of vibration control and advantages of each method, and the aim and objectives of the research are also presented in the chapter.

Chapter 2: The principles of smart fluids, previous applications and quasi static and dynamic modelling of smart fluid are also reviewed; the chapter ends with a literature review on the control methods of smart fluid devices.

Chapter 3: This chapter introduces the concept of a McKibben actuator, previous applications and methods of modelling of these materials respectively.

Chapter 4: The experimental work is shown in this chapter, which includes: designing the test rig, a basic model of a rig made of McKibben actuator and improvements to the basic model. It also provides the validation of the model under static load experimentally.

Chapter 5: This is the last chapter which provides the conclusions of this research and future work.

CHAPTER 2: LITERATURE REVIEW OF SMART FLUIDS

2-1 Background

Smart fluids are non-colloidal suspensions of magnetisable/electrical particles that are of the order of tens of microns (20-50 microns) in diameter. The formulation of Electrorheological fluid (ER) was described by Willis Winslow who achieved a US patent regarding these fluids in 1947, while Magnetorheological fluid (MR) was developed by Jacob Rabinow at the US National Bureau of Standards in the late 1940s [21]. There was a flurry of interest in these fluids during the 1950s, but this interest quickly waned, probably due to difficulties in preventing abrasion and particle sedimentation within the fluid [22]. There was a resurgence in smart fluid research that was primarily due to Lord Corporation's research and development, which succeeded in launching several commercial devices in the 1990s [23].

One of the earliest commercial devices that used MR fluid was an MR fluid brake in 1995, which was used in the exercise industry [24]. For vibration control, an MR fluid damper for truck seat suspension was introduced [10], as well as an MR fluid shock absorber for oval track automobile racing [10]. Lord Corporation has also developed a special MR fluid that will never settle out, and this damper is used in the stabilization of buildings during earthquakes [10].

Apparently, MR fluid has received significant commercial success, while ER fluid is still in the prototype stage. The reasons for this can be explained by considering the relative merits of ER and MR fluids [10, 24]. These relative merits are illustrated below:

- Although the power requirements of ER fluid and MR devices are similar (about 50 w), the value of the operating voltage is extremely varied. An ER device is required to be supplied with high voltage (2-5 KV), while MR fluid is excited by a magnetic field, which requires a low voltage source (12-24V). This low voltage is the biggest advantage for preferring g MR fluid over ER fluid.
- MR fluid is capable of generating yield stress much higher than yield stress generated by ER fluid. MR fluid could generate a dynamic yield stress of 100 kPa, while generating yield stress by ER is in the range of 3-5 kPa.
- For sensitising of temperature, the effect of temperature in MR fluid is less remarkable than ER fluid. MR fluids have a wider range of operating temperatures. MR is used from $-40^0\mathrm{C}$ to $150^0\mathrm{C}$ with only slight differences in yield stress.

- The advantage of ER is design easier than MR devices; the ER device is not requiring designing magnetic circuit, while MR device is requiring once.

Clearly, MR fluid has greater potential for commercial exploitation, so this research will focus on MR fluid more than ER fluid.

2-2 Smart Fluid Devices

A variety of smart fluids have been introduced in both research and commerce. Basically, these devices use one of three basic modes of operation: flow mode, shear mode, and squeeze mode. Moreover, any combination of these modes could be used depending on the function of the system. The first mode is flow mode, which is also called valve mode and it is a most important fundamental configuration of smart fluid devices. The fluid is forced to flow between two fixed electrode/poles, as illustrated in Figure 2-1. The applied field acts as a flow control valve, and the execution of these devices can be adjusted via control of an electric/magnetic field, which is vertical to flow direction. This type is widely used in many applications such as damping devices, actuators and prosthesis devices [10, 25].

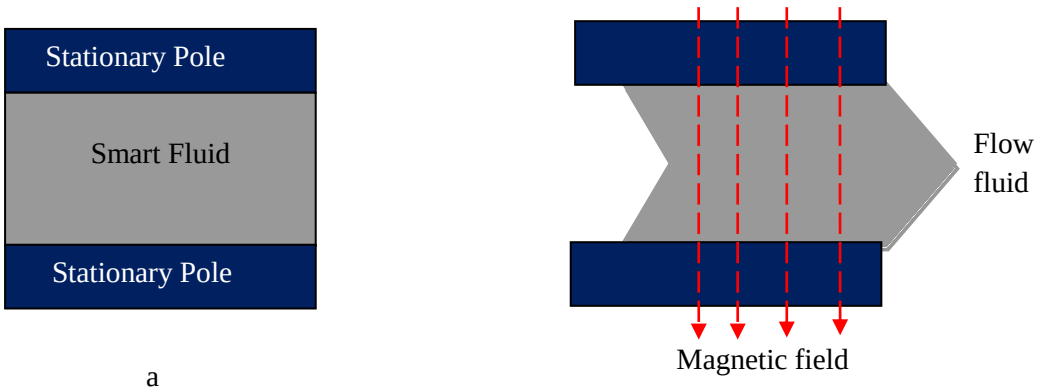

Figure 2-1: Concept of flow device: (a) without magnetic field. (b) by magnetic field.

The second mode is a shear mode; the movement type of this mode is shown in Figure 2-2, the fluid is located between two electrodes or poles, whereby only one electrode moves in relation to the other. This movement of the electrode can be either translational or rotational, and a magnetic field is applied perpendicularly to the direction of motion of these shear surfaces. Shear mode MR dampers can be carried out using three different configurations: translational linear motion, rotational disk motion, and rotational drum motion as shown in Figure 2-3. These three types of shear mode damper using Magnetorheological (MR) fluids are theoretically analyzed in [26]. Simple design and control, fast response, and simple

interface between electrical power input and mechanical output are magnificent features of the direct shear mode that make MR fluid technology suitable for many applications such as dampers, brakes, clutches and polishing devices. This model is widely used in clutches, brakes, and it is also used in dampers [27, 28].

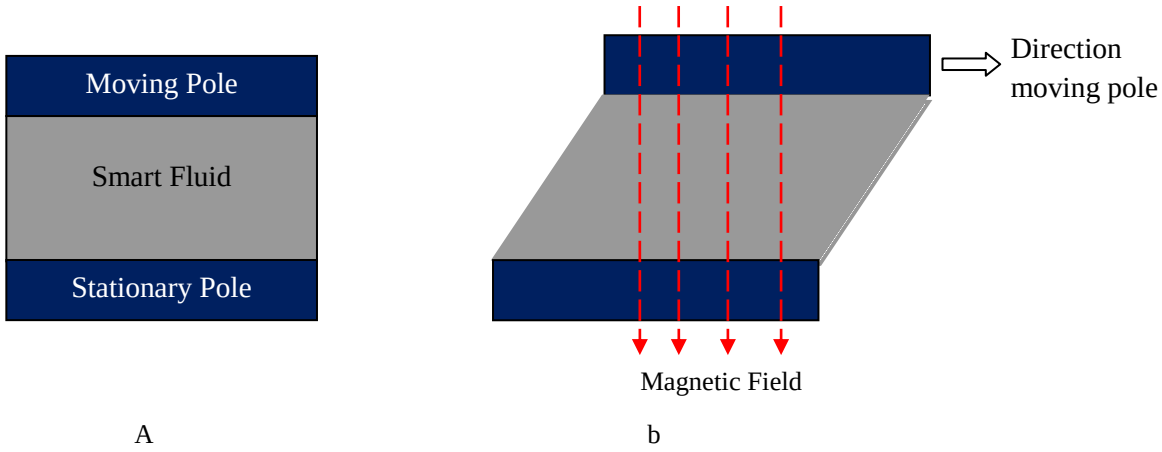

Figure 2-2: Concept of shear device: (a) without magnetic field (b) By applying magnetic field

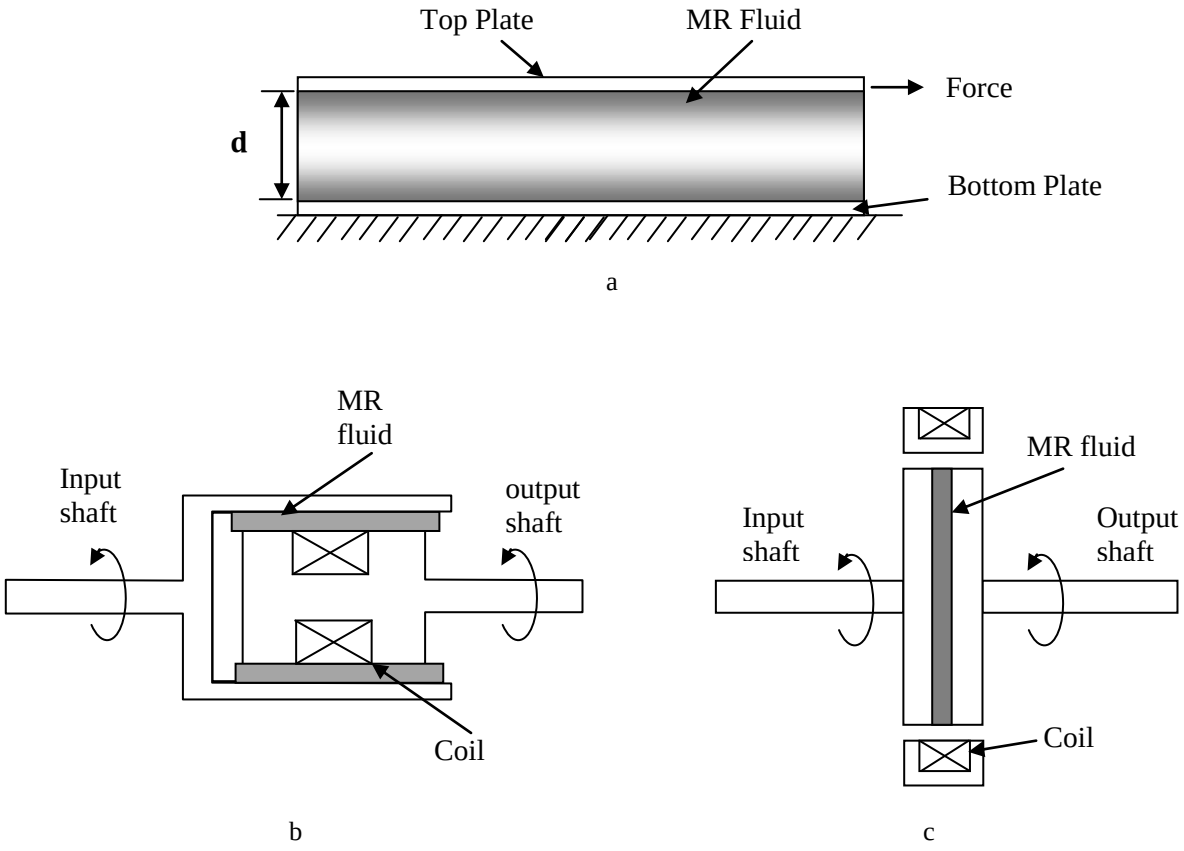

Figure 2-3: Types of Shear Mode device: (a) Liner Shear Mode, (b) Drum Shear Mode, (c) Disc Shear Mode [26].

The third working mode is the squeeze mode; it operates when a force is applied to the electrodes in the parallel direction of an applied field to decrease or increase the distance between the electrodes as it is displayed in Figure 2-4. The squeeze mode was presented by Stanway et al. [29], who found that the yield stress produced by the squeeze mode is several times greater than the yield stress produced by the shear mode. The displacements engaged in squeeze mode are relatively very small (a few millimetres) but require large forces. This is used in small applications such as anti-vibration mounts devices. Examples of this type appeared in some papers [30, 31].

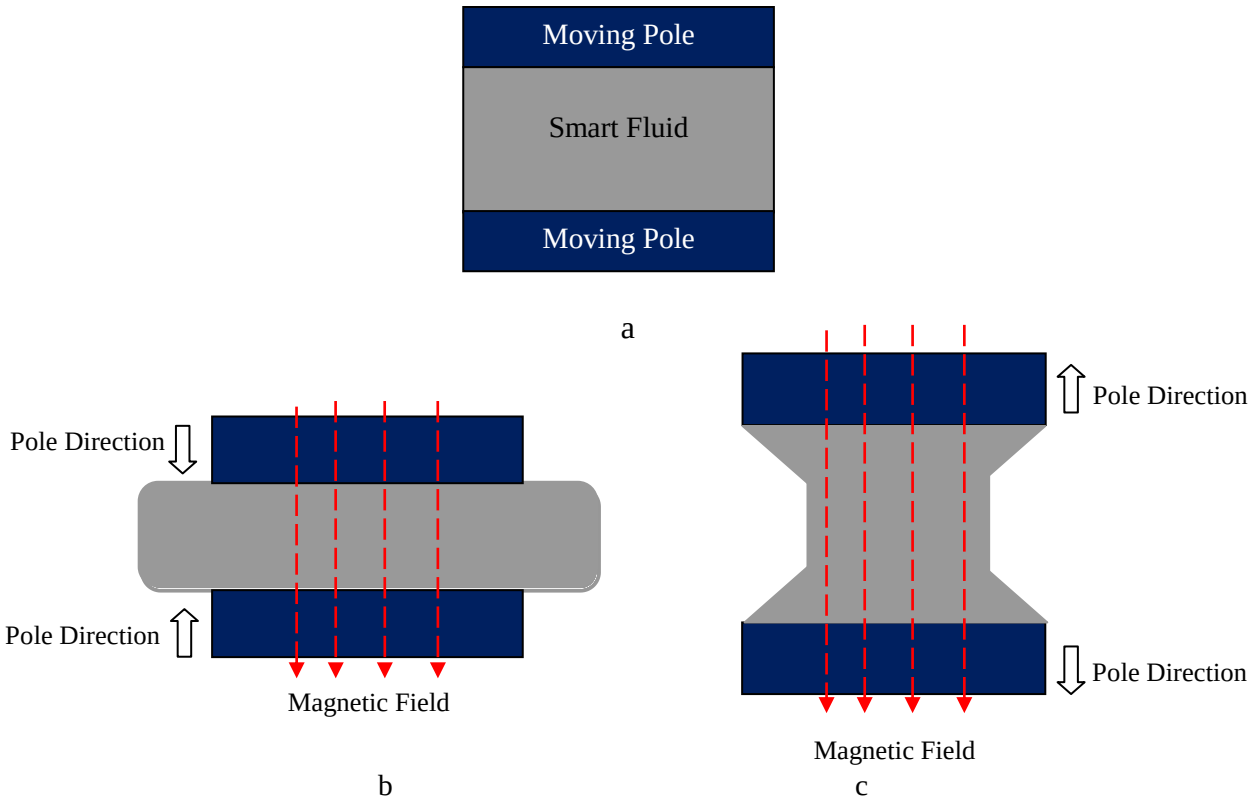

Figure 2-4 Concepts of squeeze modes: (a) Basic concept, (b) Compression in squeeze mode, (c) tension in squeeze mode.

There are also existing applications that take advantage of the combination of any two modes; shear/flow is the most common in a mixed mode device. Their combination often gives higher yield stress as compared to stress produced by individual operating modes. The piston head and cylinder wall can form the orifice of the valve; moving the piston relative to the cylinder results in a shear mode, while moving the fluid through this orifice produces a flow mode as shown in Figure 2-5 (a) [32, 33]. The combination of squeeze and shear modes of MR fluids is another experimental study introduced by Kulkarni et al. as shown in Figure 2-5

(b) [34]. The upper plate was forced to undergo simultaneous axial motion (squeeze mode) and torsional oscillations (shear mode), and the performance of the combination of squeeze and shear modes of MR fluids in dynamic loading was examined. He concluded that the yield stress is stronger if shear mode introduced the pure squeeze mode, while the introduction of squeeze can intensify or weaken the MR effect produced by the pure torsional mode.

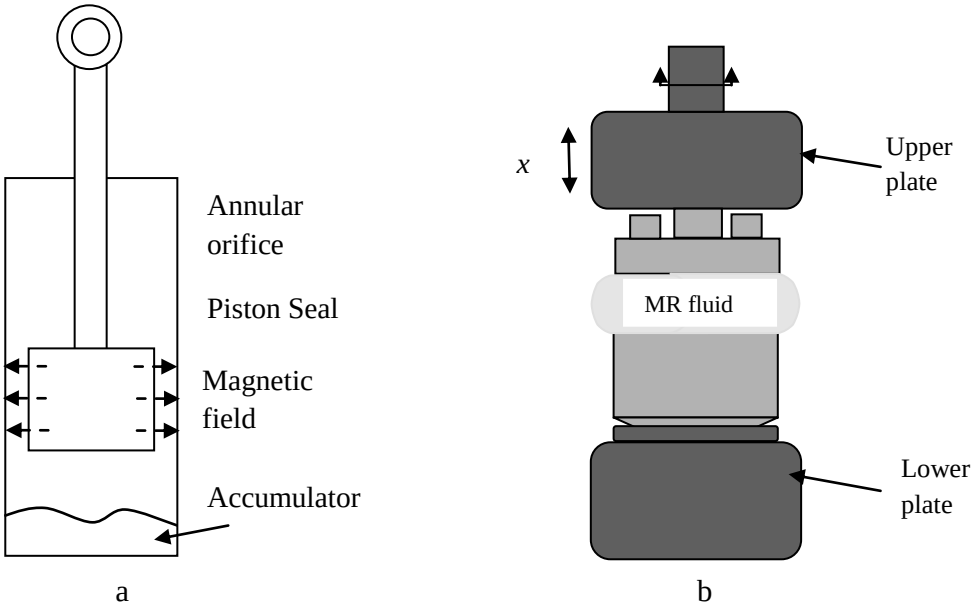

Figure 2-5: Mixed mode damper: (a) Combination of shear/flow models of MR damper [23] [33], (b) Combination of squeeze/shear modes of MR damper [34].

2-3 Smart Fluid Dampers and Mounts

The properties of smart fluids are utilized in many applications including rotary brakes, clutches, prosthetic devices, and it is even used for applications such as polishing and grinding. Among these fields, the vibration control field has been the most widely studied and developed for commercial applications. Therefore, this section will focus on smart fluid dampers and mounts.

Numerous dampers have been designed to utilize the benefits of smart fluids. These dampers can be categorized into three main types of smart fluid damper: mono tube damper, twin tube damper, and double-ended damper. The mono tube damper has one fluid reservoir, and consists of a single piston moving inside a cylinder; at the end of the cylinder there is an accumulator to accommodate the change in volume. The volume enclosed between the housing is called a reservoir of smart fluid, as shown in Figure 2-6. Commercially, this type of damper is introduced as a heavy duty vehicle seat suspension system [10].

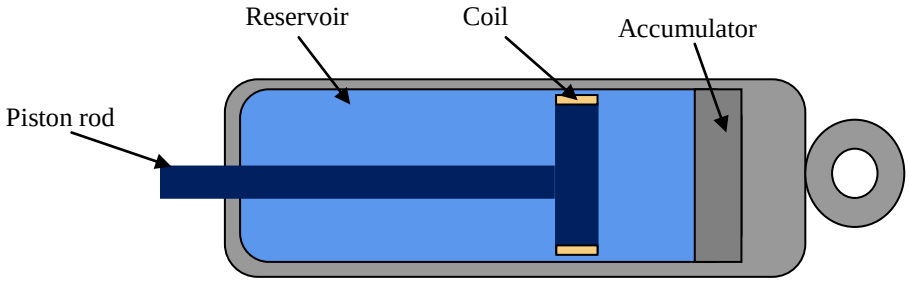

Figure 2-6 Mono tube MR damper section view [35].

There are two fluid reservoirs in a twin tube damper, one inside the other. There are also two housings, an inner and outer housing. The inner housing drives the piston rod assembly, and the volume enclosed is named as the inner reservoir in the same way as a mono tube damper. Also, the volume that is defined by the space between the inner housing and the outer housing is referred to as the outer reservoir, as shown in Figure 2-7. An example of this type, a semi-active Magnetorheological primary suspension on a heavy truck application has been designed as twin tube MR damper [36].

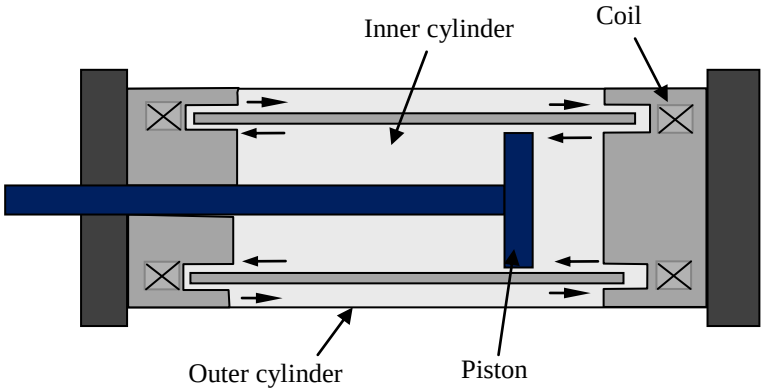

Figure 2-7 Twin tube MR damper [37].

The final type of smart damper is called a double-ended damper; the double-ended damper does not require a reservoir for changes in volume. There is a piston which is double ended inside the cylinder and this cylinder contains a magnetic circuit in some parts and during movement of the piston in this part, an effective fluid orifice is produced. Double-ended MR dampers have been used for controlling building sway motion caused by wind gusts and earthquakes , and gun recoil applications [35]. Figure 2-8 illustrates this type.

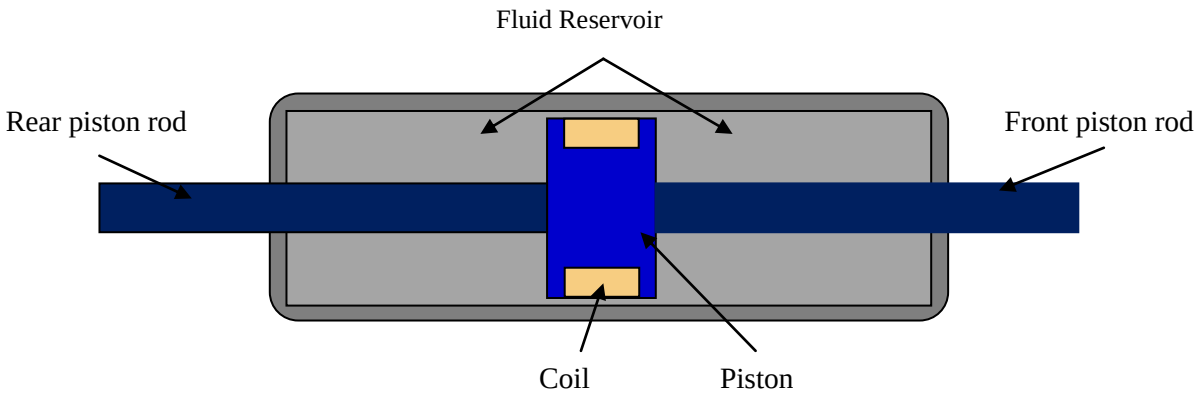

Figure 2-8 Double-ended MR damper [35].

Mounts are used to isolate sensitive equipment from vibratory sources by suppressing transmitted vibration. Usually there are no pistons in this device, and displacement levels are restricted; the prominent features of smart fluid appeared in the 1980s [38]. In the semi-active mount, the damping force can be adjusted to eliminate undesired vibration of the system by integrating variable orifice valves or fixed orifice valves, charged by field-responsive Electrorheological (ER) fluids [38] or Magnetorheological (MR) fluids [39]. An example of an isolator is shown in Figure 2-9a. This mount consists of two chambers of smart fluids connected by an ER valve and there is an inclined rubber surface on the upper chamber to suppress a static load and to pump fluid to another chamber during dynamic load, while the lower chamber ends with an accumulator to store fluid during compression [38]. Similar designs have been introduced by using MR fluids as illustrated in Figure 2-9 [39]

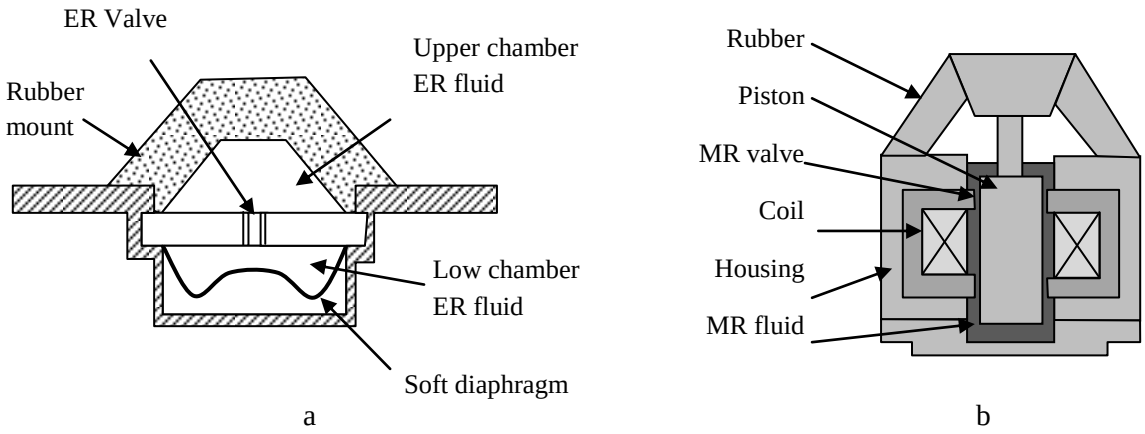

Figure 2-9: Mount of Smart Fluid. (a) ER Mount [38], (b) MR Mount [39].

2-4 Modelling of Smart Fluid

Models of smart fluid devices can be used to choose parameters that affect the design and shape of the device. They also help to improve the capability of understanding the dynamics and mechanics of the system which leads to improved performance. The dynamic responses of an MR damper under various conditions are shown in Figure 2-10 [40]. The features that are observed from the response are:

- Hysteresis phenomenon: This phenomenon is clear in a force-velocity curve Figure 2-10 (c), and its direction is anti-clockwise.
- Pre-yield and post yield: there are two rheological regions of smart fluids: pre-yield and post yield. Yield point is placed between these regions.
- Roll-off-effect: the force-velocity curve in Figure 2-10 (c) shows rapid decreasing in the velocity when the velocity is approaching zero, this is due to bleed in the fluid between the piston and cylinder which is called the roll-off effect [41].
- Passive behaviour: a smart fluid damper is considered a failsafe device, even if no current is applied; the damper has the ability to dissipate vibration as a traditional device, Figure 2-10 (a) shows that the damping force is not zero when the current is zero.

Simplicity and accuracy in results are essential in order to achieve a proper model; many researchers have presented a variety of smart fluid models. Essentially, these models are classified into two main types; the first one is a quasi-steady model which predicts the behaviour of a steady flow condition, and the second is a dynamic model which predicts the inertia and compressibility of fluid. Wang et al. also introduced other classifications, according to the modelling methods and parameters which are used. Models are divided into parametric and non-parametric, while models are divided into dynamic models and inverse dynamic models according to reversibility [11]. In this research, the first classification only quasi steady and dynamic models will be considered.

Smart fluid quasi-steady behaviour is usually described as a Bingham plastic; development and experimental validation of quasi-steady smart fluid damper models have been introduced. Various non-dimensional forms of the Bingham plastic equation have been introduced, for instance, Phillips [42] developed a set of non-dimensional variables and the corresponding equations to determine the pressure gradient through a duct. Stanway et al [38] developed an alternative non-dimensionalization scheme for flow mode dampers utilizing a friction coefficient, Reynolds number, and the Hedstrom number. Wereley and Pang [32] presented a

set of non-dimensional groups with which to characterize the equivalent viscous damping constant of smart fluid dampers; the three non-dimensional numbers are the Bingham number, the non-dimensional plug thickness, and the area coefficient which is defined as the ratio of the piston head area to the annular area between the electrodes.

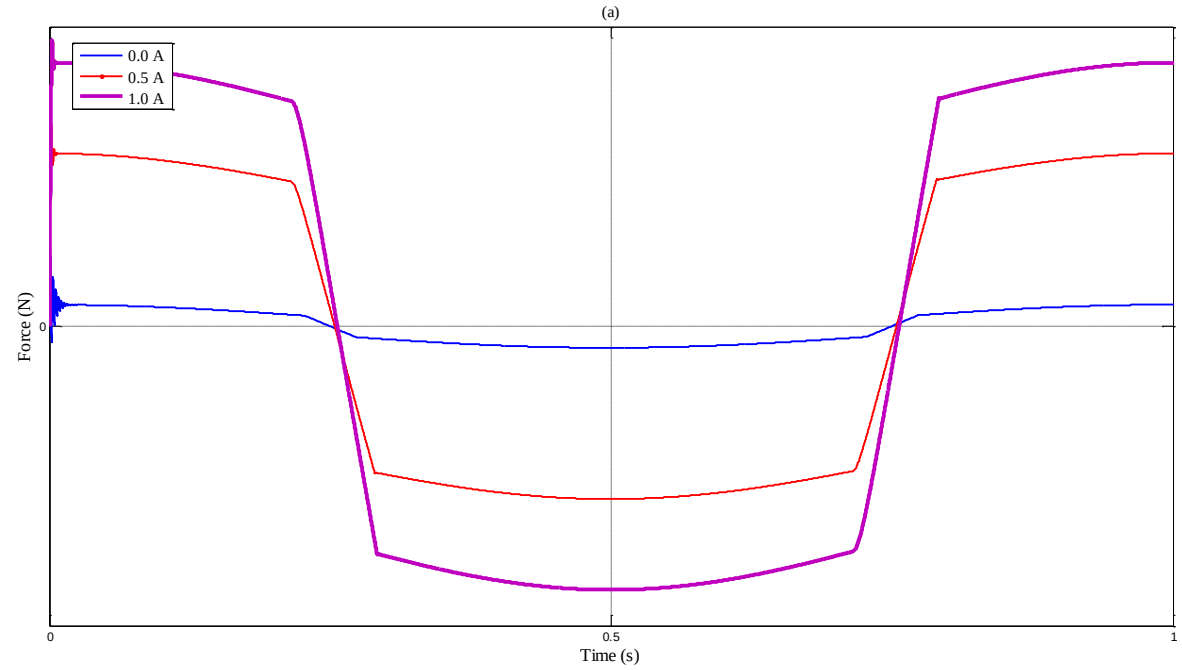

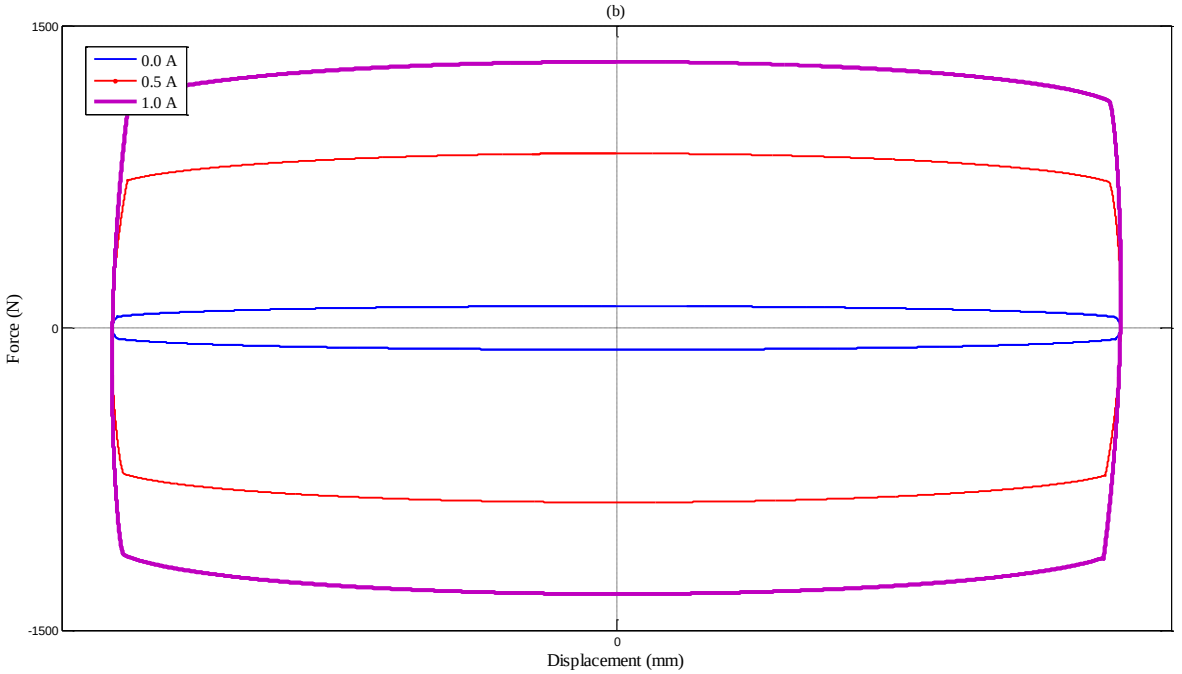

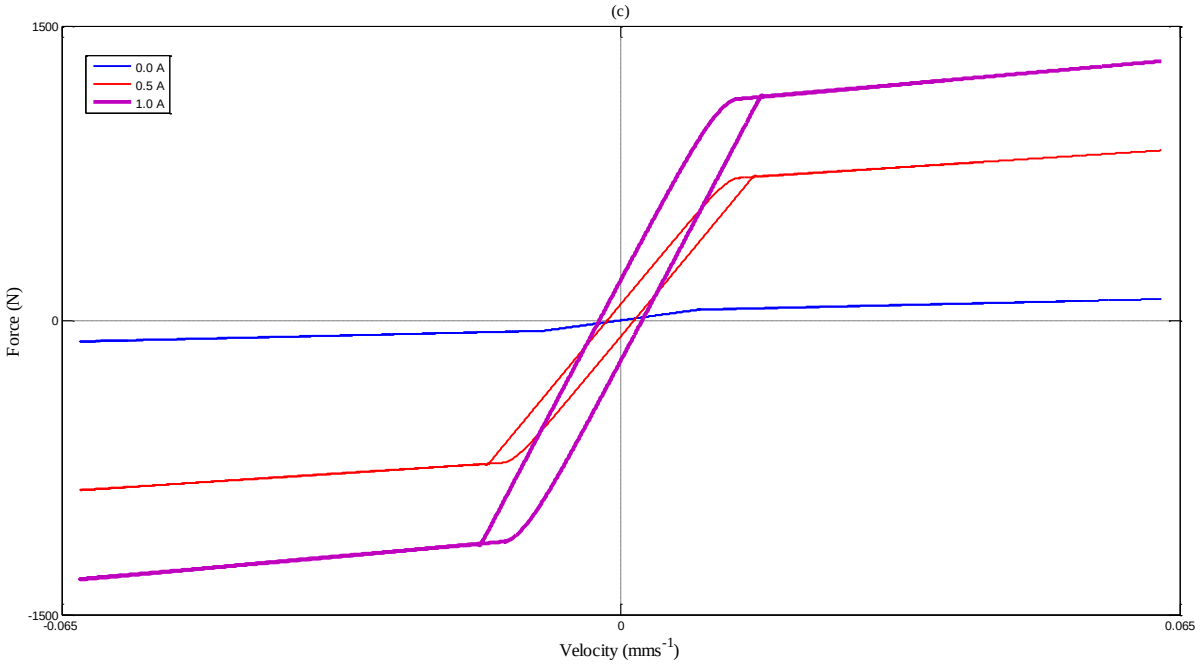

Figure 2-10 :Measured damping forces of smart fluid damper: (a) force Vs time (b) force Vs displacement, (c) force Vs velocity [40].

To simplify the quasi-steady analysis, the annular duct, which is the most common configuration of a smart fluid damper, is modelled as a parallel flat plate or rectangular duct geometry [32]. Experimentally, it was noted that smart fluid may exhibit shear thickening or shear thinning behaviour for the post yield region at high speed, and the Herschel-Bulkily model takes these changes into account [43].

For a dynamic parametric model, Gamota and Filisko [44] introduced an extended Bingham model as shown in Figure 2-11 (a). This model is based on Stanway's model (Bingham model). The Bingham model consists of a parallel arrangement of Coulomb friction elements to model the yield response and a viscous damper to model the post yield response [45]. Gamota and Filisko added viscous and elastic elements to account for the viscoelastic pre-yield behaviours. The extended Bingham model is able to give a good result for observed behaviour, but the cost of solution is significantly increased [41].

The viscoelastic–plastic model is another dynamic modelling method [46]. In this model, the response of the smart fluid is divided into two distinct rheological regions: pre-yield region where the response was viscoelastic; and a post-yield region where the response was plastic. Each region is modelled separately as shown in Figure 2-11 (b). The pre-yield region exhibits a strong hysteresis, which is typical of a viscoelastic material. This is modelled as the Kelvin chain element which can be represented by a viscous damper and elastic spring

connected in parallel [47]. The post-yield region is plastic with a nonzero yield force, as in the nonlinear Bingham plastic. It can be modelled as a viscous damper [37]. Some researchers added other region. Yield region is located between two previous regions; the response of yield region is viscoelastic–plastic. The yield force is a function of the applied field and is a field-dependent parameter that provides the damper with semi-active capabilities.

Spencer introduced the Bouc-Wen model [41]. This model is based on the analysis of the Bouc-Wen model of hysteresis behaviour, and then damper and spring are added to the basic configuration being shown in Figure 2-11 (c). A reasonable predication of force-displacement was achieved in this model; however the force-velocity curve does not give reliable results, especially in the roll-off-effect in the yield region. To get significant accuracy, additional parameters are added to an improved model as shown in Figure 2-11 (d), the degree freedom of system is also increased, the result is improved. this model has been validated in a variety of conditions [41]. Similar to the former model, several mathematical expressions that capture hysteresis behaviours have been modified, for instance: the Dahl model which used the Dahl expression [48], and the hyperbolic tangent function-based model presented by Kwok et al [49] which used a hyperbolic tangent function and linear functions. These models may predict a reliable result, but their drawbacks are that the identification of a large number of parameters is essential.

Sims et al. introduced a new model based upon fluid properties and device geometry. It is composed of: a quasi-steady damping function that can be derived from an analytical model; mass that to represent fluid inertia; a spring that to represent fluid compressibility; and another mass to represent the piston head. All parameters are linked in series as shown in Figure 2-11 (e) [50]. The advantages of this model are that its parameters can initially be determined based upon constitutive relationships using fluid properties and device geometry rather than using observed experimental behaviour. Therefore, an accurate dynamic model can be developed before the manufacturing process.

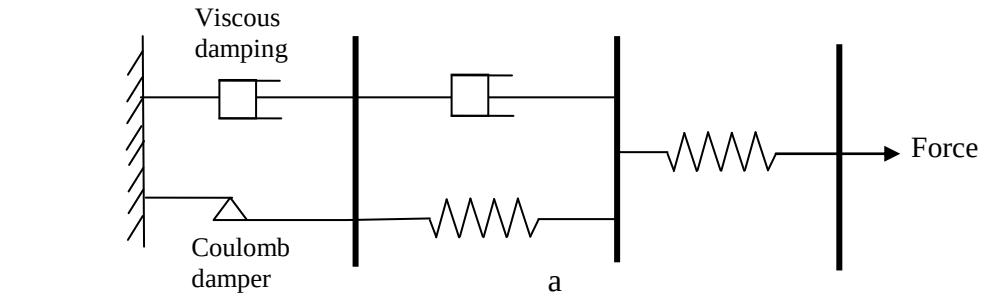

a

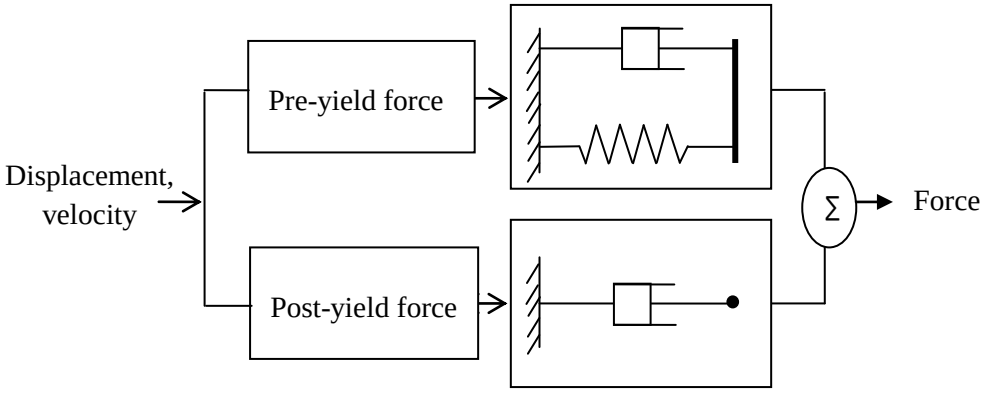

b

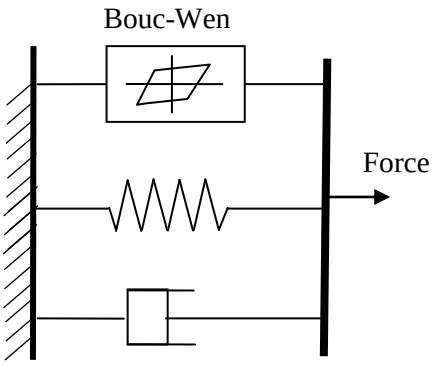

c

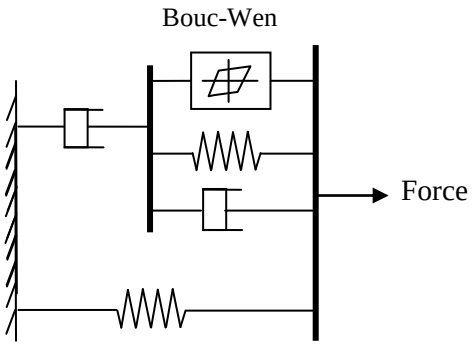

d

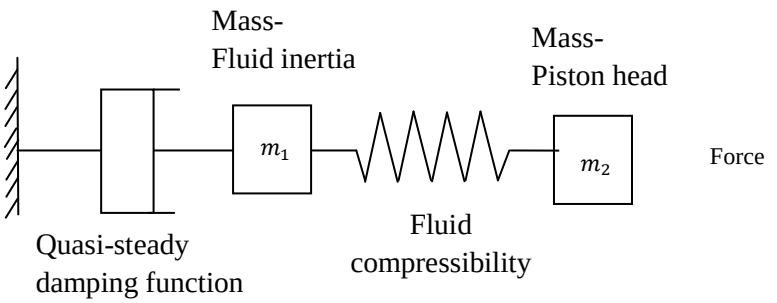

e

Figure 2-11: Dynamic modeling of smart fluid. (a) extended Bingham model, (b) viscoelastic-plastic model, (c) Bouc-Wen model, (d) extended Bouc-Wen model, (e) Sims' Model [11].

2-5 Control of Smart Fluid

Similar to modelling of smart fluid, it is difficult to achieve reliable control systems due to inherent hysteresis behaviour. To design efficient controllers, it is required that two main objectives are obtained: the first objective is to calculate an input voltage; and the second objective is to determine the output of the device which is a damping force. The non-linear behaviour of smart fluid dampers makes the objective of achieving a desired force very difficult. The MR damper based semi-active control system consists of a system controller and a damper controller, as shown schematically in Figure 2-12. The system controller generates the desired damping force given system conditions. Another controller (damper controller) sets the command voltage to the current driver, to track the appropriated damping force. The damping force of the MR damper should be predicted and fed to the damper controller to generate the command voltage according to the desired damping force generated by the system controller. So the predicting damping force and the generating command voltage are the two main objectives to control a smart fluid damper [51].

There are a wide range of control strategies (experimental and theoretical) that have been adopted in order to calculate the desired damping force, for example: the clipped-optimal control strategy has been used to control a story test structure, and excellent results have been achieved; neural network control methods applied to a quarter car model with an MR damper [52]; and fuzzy logical strategy has been applied in quarter car model of a 70-ton rail car [53].

Many of the control strategies have tracked the force by linearization between input (current) and output (damping force) [54]. Other researchers simplify the force tracking strategy by using on/off where the applied voltage is either 0 or maximum [55]. The feedback linearization strategy has been pursued by scholars; this approach can obtain an accurate set-point force without suffering from a variation of parameters [56].

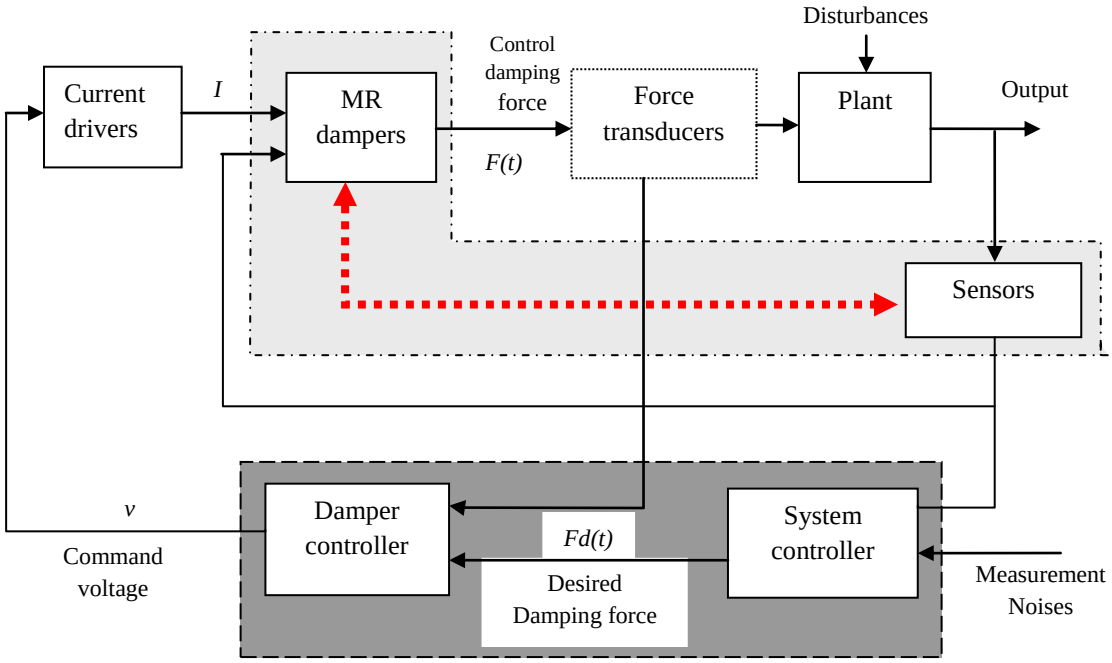

Figure 2-12: Schematic of the MR-damper-based semi-active system [51].

2-6 Summary of the chapter:

This chapter contains the literature survey on the smart fluids. It starts by describing the concept of smart fluid and making a comparison between two types of smart fluids: Electrorheological fluid (ER); and Magnetorheological fluid (MR). The various modes of smart fluid configurations are then described, and application of semi-active damping devices, which include dampers and mounts. The survey also included models of a smart fluid damper; the quasi-static models which are used to predict the behaviour of flow fluid and used to design the prototype of a device, and dynamic models which predict the compressibility and inertia of fluid, which are used to design the control strategy of smart fluid devices. A review of smart fluid is concluded by control strategies used for smart fluid dampers.

CHAPTER 3: LITERATURE REVIEW OF McKIBBEN ACTUATOR

3-1 Background

The McKibben actuator is a device that can convert fluid pressure fluid to force. It consists of an internal rubber tube inside a flexible matrix composite tube. The flexible matrix composite tube (FMC) consists of two families of oriented stiffening fibres (braided fibres) that can achieve flexibility in certain directions and is strong in other loading directions. When the inner tube is inflated by pressurized air, the volume of the tube will be increased, causing constriction in the length of the actuator. In the same manner, reducing internal pressure of the tube will lead to minimizing the volume and to expanding the length of the tube. The earliest reference of a braided pneumatic actuator was introduced by Robert Pierce in 1936 [6]. His device was invented to utilize from expanding the tube in the radius direction in the mining industry, but he did not mention changing of the tube in the axial direction. This led R Gaylord to patent a fluid actuated motor and stroking device in 1958 by introduced the device utilizing longitudinal contraction. This actuator is called a pneumatic muscle. The physicist J. L. McKibben popularized its use when he used it to activate orthotic devices for upper extremities in the 1950s. Since that time the device become known as McKibben muscles. The pneumatic muscle entered into the robotic industry in the 1980s, with the development of a commercial version of the pneumatic muscle used in industrial robotic arms. A new structure was introduced in 2006, called a fluidic flexible matrix composite F^2MC. It has a similar structure to McKibben actuator, and it consists of the flexible matrix composite tube (FMC) and inner rubber tube. However, fibres in an FMC actuator can be located at any one angle or combination of angles, whereas fibres in a McKibben actuator are generally restricted to equal and opposite angles, therefore the FMC structure is able to generate a higher output force compared to a McKibben actuator [57].

This chapter will present previous devices that have been made of McKibben actuator. Operation methods of these actuators will also be presented. In the final section, methods of modelling these materials under static and dynamic load will be introduced.

3-2 McKibben Devices

There are lots of applications made from McKibben actuator introduced commercially or in research. These applications could be divided into two main types, depending on the working

fluid inside these materials: air such as a pneumatic actuator or McKibben muscle, and water in hydraulic muscles and fluidic flexible matrix composite F^2MC applications.

The devices that use pneumatics in a flexible matrix composite are known as a pneumatic muscle actuator (PMA) or McKibben actuator, which is a device that mimics the behaviour of skeletal muscle. Many different fields are utilizing this device. Since McKibben introduced this actuator as an artificial muscle for his daughter, and due to the inherent safety and high power to weight ratio provided by the pneumatic muscle, the majority of McKibben actuators introduced are used in human interactions such as a prostheses, rehabilitation and mobility assistance. Examples of these applications are: a gait assistance device which is able assist and improve the muscular activities of the elderly, with the research analysing the flexing and extending movement of the knees, and the lower limbs muscles [58]. A hand therapy device made of a pneumatic muscle has been developed, to assist disabled people, and the cost of this device is cheaper than intensive repetitive therapy [16]. A lightweight device operated by a pneumatic actuator used in both upper and lower body rehabilitation was developed; this device provides systems with reasonable power and control as well as safety for the user [59]. Several groups of researchers are using pneumatic muscles as actuators in robotic devices such as whole body humanoids, robotic arms or bipedal robots, moreover pneumatic muscle is also used to model some animals and insects [6]. Pneumatic actuators also have some applications in industrial fields such as tele-operated actuator which used in nuclear reactors [17]. Recently, some morphing applications made from McKibben actuator has been studied, Chen et al. used a pneumatic actuator to design a kind of morphing skin; the experiment concluded that the contraction ratio of the device is up to 26.8% [60].

Commercially, the Bridgestone Rubber Company for Robotic Applications introduced the first McKibben muscle called Rubbertuator [61]. Other companies used different names, for instance: The Festo Corporation marketed fluidic muscle [6, 62], and the Hitachi Medical Corporation called their product McKibben Muscles [6].

Using hydraulic working fluid (e.g. water) in a McKibben actuator is quite a new application. The working fluid in exoskeleton devices and devices working in a water medium is usually water. For instance: an actuator for an underwater robot was introduced by Kenneth et al. [18], and haptic gloves that are able to produce up to 5 N have been presented by Ryu et al [63]. Shan et al. developed a variable stiffness adaptive structure that could be used in

morphing applications [19]. They used material called fluidic flexible matrix composite materials (F^2MC) which has a similar structure to a McKibben actuator. However, fibres in an F^2MC structure can be placed at any one angle or combination of angles. There are several applications presented using F^2MC Materials. For example, Li and others researched using a fluidic flexible matrix composite in a honeycomb sandwich structure. This has been done by replacing the upper sheets in a traditional sandwich structure with an adaptive structure made of fluidic flexible matrix composite tubes [64]. For medical equipment, this material is investigated in prosthetic and orthotic devices, and is used to minimize the load transfer between the limb and transtibial socket for amputees. This has been done by a valve control of the variable impedance (F^2MC) system [65]. For dissipated vibration devices, a tuned vibration absorber is designed by coupling a fluidic flexible matrix composite to fluid motion [66], while Philen introduced a mount made of a fluidic flexible matrix composite [67].

3-3 Driving Methods of McKibben Devices

Although the majority of McKibben actuators introduced are driven by pressured air, there are other techniques. Following is a brief presentation of the operation techniques of a McKibben actuator:

1- Actuator drive by air pressure: Most pressurized artificial muscles are driven by air. A pneumatic McKibben actuator driven by air requires pressure ranging 0–6 bar, while a hydraulic McKibben actuator requires higher pressure which could reach 100 bar, however it is generating a higher force [68].

2- Actuator drive by chemical process: A McKibben actuator driven by a chemical process has been developed [69]. They used pH-sensitive materials, an ion-exchange resin and Sodium Hydroxide/Hydrogen chloride (NaOH/HCl) solutions; the introduced device could produce 100N.

3- Actuator drives by electro-conjugate: An electro-conjugate fluid (ECF) is a type of dielectric functional fluid, which when a high DC voltage is applied, a powerful jet flow is generated between two electrodes; this smart fluid has been used to drive the McKibben actuator [70].

3-4 Modelling of McKibben Actuator

There have been many efforts to model the behaviour of a McKibben actuator, aiming to gain a deeper understanding of its behaviour and to shape the foundation of a control system.

Much of the past work on McKibben muscles has been focused on modelling the resulting force and its behaviour accurately. High deformation and nonlinear behaviour of the actuator cause difficulty in producing a highly accurate model. In this section, the static and dynamic models are reviewed and presented.

3-4-1 Static Model

According to the literature, three approaches were introduced for modeling the response of a McKibben actuator. These models are; virtual work; force analysis; and the continuum mechanics.

The virtual work principle which is based on the input work being equal to the output work was applied by Chou and Hannaford [71]. It is the oldest and the most wide spread approach used for modelling a McKibben actuator. The McKibben muscle actuator consists of an internal tube made of rubber inside a braided mesh shell; when the inner tube is inflated, the internal volume will increase; increasing the internal volume causes the actuator to expand in the radial direction and contract in the longitudinal direction. By considering the following assumptions; no energy is stored in its elastic wall, and the actuator has a cylindrical shape. The resulting equation of this model linked between the internal pressure and the resulting force:

$$F = \frac{\pi D^2 P^{'}}{4}(3\cos^2\theta - 1) \qquad 3\text{-}1$$

Where: F is a contractile force, P' is a gage pressure, D is a diameter of the tube and θ is a fibre's angle. Other researchers also concluded the same equation such as: Caldwell et al [72] and Tasagarakis et al [73]. There are of a lot of publications that refer to Schulte as the first person to introduce this equation in 1963 [6, 74]. Due to several assumptions and ignoring several parameters, this model may not reach high precision. According to Davis et al [61],the accuracy of this model is about 80-90%, while Doumit claims validation of this model is rarely true [75]. Subsequently several scholars have extended this model by taking into account more realistic assumptions. Chau and Hannaford took the effect of the thickness of an McKibben tube into their analysis [76] giving:

$$F = \frac{\pi D^2 P'}{4}(3\cos^2\theta - 1) + \pi P'(D t_k\left(2\sin\theta - \frac{1}{\sin\theta}\right) - t_k^2) \qquad 3\text{-}2$$

t_k Thickness of McKibben tube, F is an output force, P' is a gage pressure, D is a diameter of the tube, and θ the fibre's angle.

Tondu and Lopez introduced a new element k, which represents the conic shape that occurs at both ends of the muscle when it contracts in the pneumatic muscles. The value of the new parameter k is estimated on the basis of experimental data [77].

$$F = \frac{\pi D^2 P'}{4}[a(1-k\varepsilon)^2 - b] \quad 3\text{-}3$$

Whereas: $a = \frac{3}{\tan^2\theta}$, $b = \frac{1}{\sin^2\theta}$, and $\varepsilon = \frac{L_0 - L}{L_0}$

L_0 and L are an unstrained length and instantaneous length of McKibben tube.

Colbrunn et al. presented the model in terms of length of coiled fibre and length of uncoiled fibre instead of the fibres' angle, because it is not easy to measure the angle experimentally. They also added end effects which change the force at the maximum and minimum length. When the actuator reaches the maximum length $L_{\max}$, stretching in the fibre will occur, therefore the force will be dependant on the material of the fibre. The force is zero if the length of the actuator is less than minimum length $L_{\min}$, their model is shown in the next equations [78].

$$F = \begin{cases} \frac{P' b^2}{4\pi n}\left(\frac{3L^2}{b^2} - 1\right) + F_{max} & if\ (L > L_{\min}) \\ 0 & if\ (L < L_{\min}) \end{cases} \quad 3\text{-}4$$

Where:

$$F_{max} = \begin{cases} K_{\text{fiber}}(L - L_{max}) & if\ (L > L_{\max}) \\ 0 & if\ (L < L_{\max}) \end{cases} \quad 3\text{-}5$$

Where: b length of uncoiled fibre, n number of turns, K_{fiber} stiffness of fibre material, D is a diameter of the tube and is the θ fibre's angle. Tsagarakis and Caldwell considered the conical shape at the end of device in their analysis [73], and considered the shape of the actuator as cylindrical in the middle and conical at the tips. They claimed the model raises the accuracy by 30-50%. Klute and Hannaford [79] improved the model by calculating the effect of the strain energy storage in the elastic inner tube which is made of rubber. It was assumed that the bladder was thin and made of Mooney–Rivlin material. Sugimoto et al. calculated the strain energy density function by the main strain variables [80].

Many of these virtual work models contain experimentally determined parameters, including parameters taken from experiments on specific devices, leading to validation only for a specific pneumatic muscle. In order to remedy this limitation, Doumit et al. introduced a model to overcome this issue; they used force and stress analyses to present a static model that is valid for any pneumatic actuator size and configuration. This model considers the

mechanical properties of the inner tube, and netting analysis of the braid were also considered in the model [75]. The properties of the inner tubes were determined via a tensile test. The material properties along the longitudinal axis of the bladder are of less consequence, so it is not considered; only hoop stress is considered. The braided mesh properties which are considered have a cylindrical shape in the middle and a conic shape at both ends. The muscle wall stresses that act on the braid fibres produce a tensile force in them. The tension in these fibres acts on the end cap to produce the muscle force.

The third method of modelling a McKibben actuator is a continuum mechanics approach, which has been proposed by Liu and Rahn [81]. The McKibben actuator was modelled as a large deformation membrane with two families of continuously distributed inextensible fibre reinforcement. Although this approach would obtain more accurate of actuator shape, the difficulty of solving the differential equations, which is a boundary value problem, is the main disadvantage of this model.

3-4-2 Dynamic Modelling

The dynamic model of the McKibben actuator is extremely difficult to develop due to its nonlinear behaviour, the large deformations, and the internal damping.

Sugimoto et al. including the damping force in the static model to get a dynamic force output of the McKibben actuator; the damping force is supposed as a function of only velocity [80].

Chou and Hannaford were interested in predicting the behaviour of the internal fluid pressure and mass flow. Their model was an electrical circuit which is analogous to the pneumatic circuit. The difference of pressure in actuator $P_1$and pressure accumulator P_2 is analogous to the voltage difference between two nodes. The gas flow is equivalent to the current. The gas viscosity caused by the tubing and the connections was modelled as a linear resistor R, and the accumulator was modeled as a linear capacitor [76].

Colbrunn et al introduced a phenomenological model which aimed to better capture the dynamic behaviour of pneumatic muscles. The pneumatic muscle model consisted of a spring, viscous damper and Coulomb friction element arranged in parallel as shown in Figure 3-1 [78]. The spring represents the nonlinear force-length relationship, a viscous damper represents the fluid flow losses, and the Coulomb friction represents the friction between the internal bladder and outer braided shell:

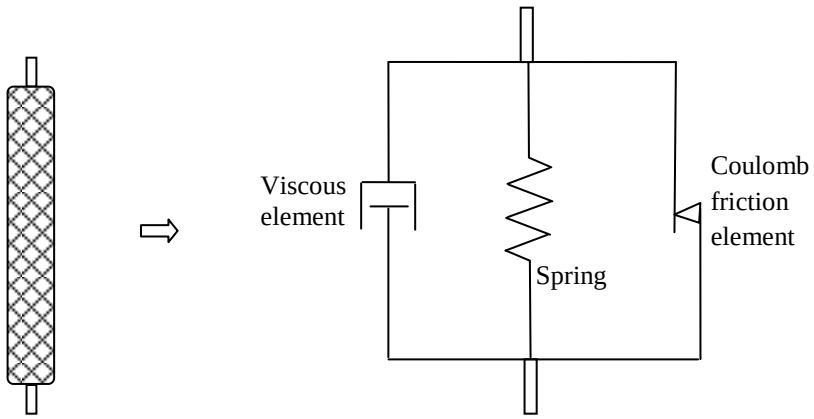

Figure 3-1: Phenomenological model of McKibben actuator

$$F = \frac{P'b^2}{4\pi n^2}\left(\frac{3L^2}{b^2} - 1\right) + cv \pm Qk \qquad 3\text{-}6$$

Where: c is the viscous damping constant, v actuator velocity at the top, k is linearization actuator stiffness, and $Q = \frac{\mu N}{k}$ is a Coulomb damping constant.

Reynolds et al.[82] developed another phenomenological model consisting of a spring element, viscous damping element, and contractile force element arranged in parallel as shown in figure 3-2. The spring coefficient was taken to be a function of position and the damping coefficient a function of velocity. All these parameters are found experimentally. While the contractile force element varied with internal pressure and the length of tube, the contractile force was calculated by using next expression:

$$F_{ce} = \frac{P'b^2}{4\pi n^2}\left(\frac{3L^2}{b^2} - 1\right) \qquad 3\text{-}7$$

Where: F_{ce} is a contractile force, P' is a gage pressure, b length of uncoiled fibre, n number of turns, and L is a length of the tube.

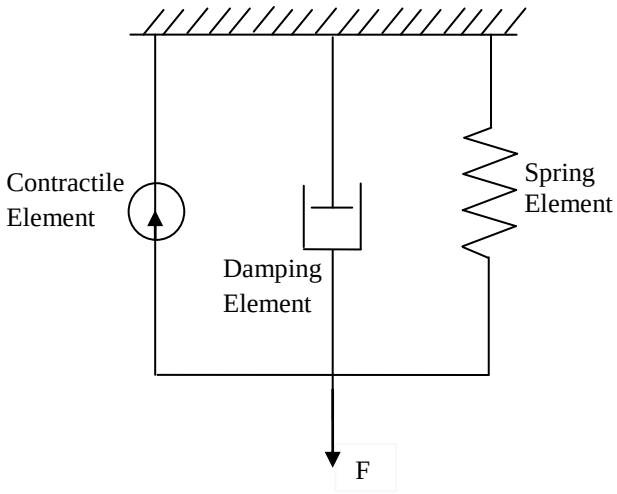

Figure 3-2: Reynolds model of McKibben actuator

3-5 Summary of the Chapter

In this chapter the idea of a McKibben actuator is presented. The concept of a McKibben actuator with its history is summarized briefly for the background. Then the second section of the survey presented the previous devices of the McKibben actuator and its applications. The previous applications of a McKibben actuator were driven by various methods, therefore these methods were studied. The last part of the review contains the previous methods of modelling a McKibben actuator: this includes static models that are used to design the device in the manufacturing process, and dynamic models which help to find the control strategies of the device.

CHAPTER 4: DESIGN OF THE TEST FACILITY

4-1 Introduction

As mentioned in the literature review chapters, semi active vibration control is an attractive technique for vibration control. It is also mentioned that smart fluid is one of most superior means of control of the vibration [8], and there are a lot of semi-active applications that profit from the characteristics of smart fluid, when employed successfully [83]. However, the conventional MR dampers have a dry seal friction. This friction makes a tiny vibration transmission to equipment; therefore, this tiny vibration may badly affect sensitive devices[13].

To reducing influence of friction, the possibility of design MR damper by using McKibben actuator will investigated. Although McKibben actuator has been used in human interaction devices since the 1950s, the variable damping behaviour of this actuator was only noticed recently. Therefore, several applications in semi-active vibration control have appeared [84]. McKibben actuator has other advantages over the hydraulic and cylinder actuators such as: light weight and low cost maintenance. To understand the behaviour of McKibben actuator, and how it behaves under loads, the McKibben actuator will be designed and tested. In this research, the working fluid of the McKibben tube will be water; studying the behaviours of this tube by using water is an initial step before using smart fluid, as it will give a good ground to establish a McKibben damper when using smart fluid.

This chapter will deal with the design of a McKibben actuator, and then the behaviour of this tube under static load will be predicted. The chapter will end with the validation of this prediction experimentally.

4-2 Test Rig (McKibben Actuator)

A McKibben actuator is used to convert internal pressure to linear force. The test rig used in this research consists of: a McKibben tube, valve and pressurized accumulator as shown in Figure 4-1. The McKibben tube consists of a rubber tube surrounded by an expansible braided cover. The McKibben tube is sealed at one end, and it is able to carry load at this tip, while the tube is attached to an accumulator via a ball valve at another end. The test rig is

fixed in a frame to be fixed during the process of the experiments. The frame is covered to protect electrical devices in case of tube explosion at high pressure. Pressurizing the McKibben tube could be achieved by using a pump through a Schrader valve located at the top of the accumulator. The pump is connected to a gage pressure to measure the pressure of the accumulator and inside the McKibben actuator in case of an open valve. There is an additional digital gage pressure installed between the McKibben tube and ball valve to measure the pressure in case of a closed valve. The idea of this device is: applying force to the end of the test rig will change the volume of the McKibben tube, and consequently the pressure will be increased inside the tube. Then, the fluid is able to flow in and out of the tube, and energy will be eliminated through the viscous effect of the controlled valve (magnetic effect in the case of using an MR valve). Similar to this, a damper was introduced by using a Fluids Flexible Matrix Composite F^2MC material [7].

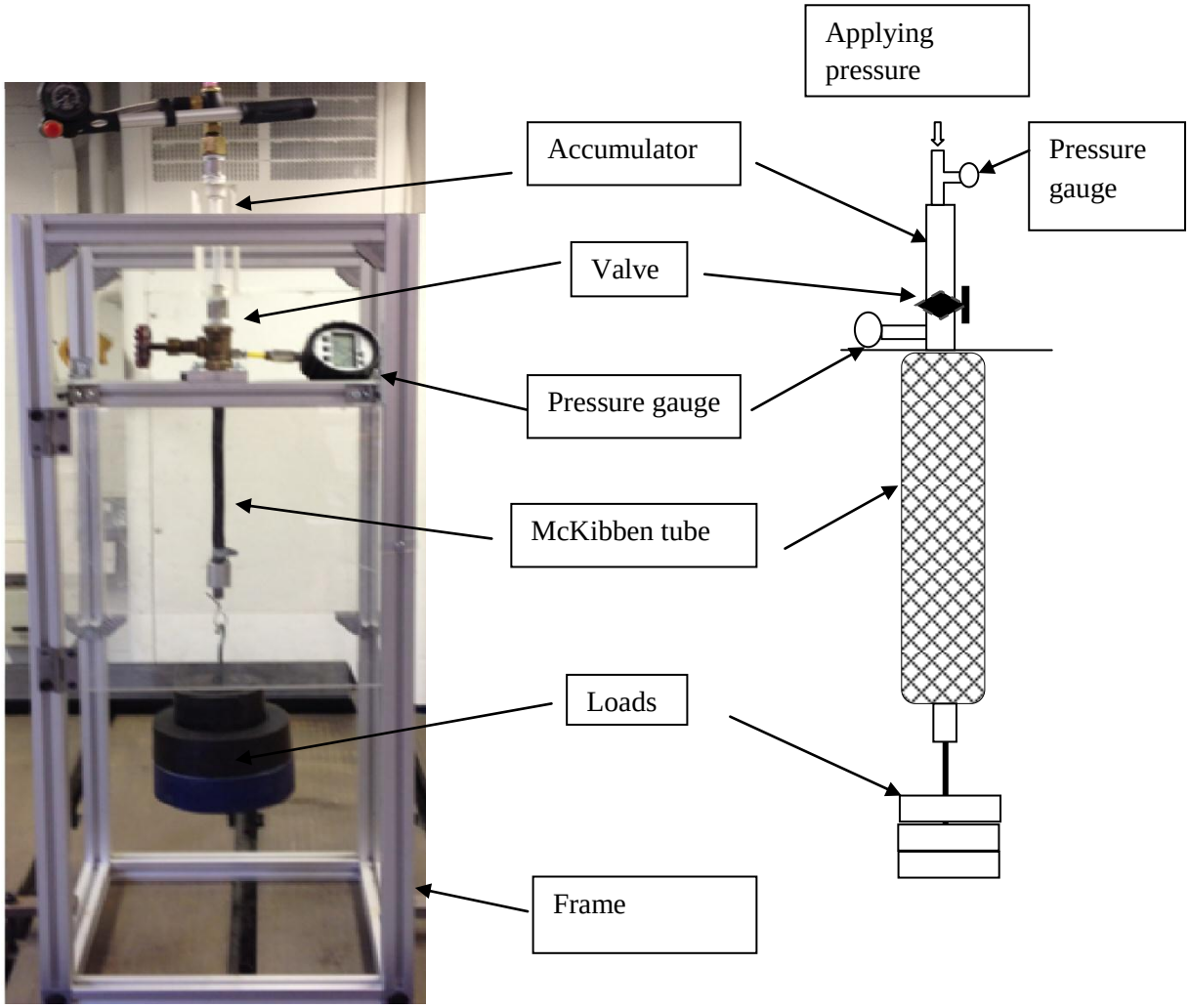

a b

Figure 4-1: Test rig. (a) McKibben actuator, (b) Sketch McKibben actuator.

4-3 Static Model of the Test Rig

To predict the behaviour of the test rig under static load, there is no effect of viscous damping of the valve, and the test rig could be modelled similar to a McKibben actuator. There are three variable parameters of this device: a force applied to the test rig, internal pressure of the McKibben tube, and length of the McKibben tube. There are several techniques used for predicting the behaviour of this actuator and to provide a relationship between variable parameters. The technique of energy analysis, where input work (W_{in}) is equal to the output work (W_{out}), will be used in this research. The following assumptions have been considered:

- Energy stored in an inner tube (rubber tube) is zero.
- Wall thickness of the inner tube is zero.
- The shape of the McKibben tube is cylindrical.

The input work is done on this actuator by applying compressed air; this air moves the inner rubber surface, so the work is:

$$dW_{in} = P'dV \quad \text{4-1}$$

Where: dV volume change, and P' gauge pressure.

The output work from this pressure is tension in the actuator, which leads to a decrease in the length of the tube:

$$dW_{out} = -FdL \quad \text{4-2}$$

Where: F axial force, and dL axial displacement. From the principle of virtual work, we could reach to the next expression:

$$P'dV = -FdL \quad \text{4-3a}$$

Or

$$F = -P'\frac{dV}{dL} \quad \text{4-3b}$$

This equation is similar to the hydraulic cylinder equation $F = PA$; the amount of force a hydraulic cylinder can generate is equal to the hydraulic pressure times the effective area of the cylinder. Therefore, the value of dV/dL is the effective hydraulic area of the actuator.

It is difficult to find dV/dL for irregular shapes, therefore the shape of a tube is assumed as a cylindrical shape. The dimensions of this cylinder are: L is the length, D is the diameter, and the fibre angle is θ; these dimensions are changing during the applying load. The geometry has constant dimensions: b is the length of uncoiled fibre and n the number of turns for a single fibre. The relationship between these parameters is illustrated in Figure 4-2:

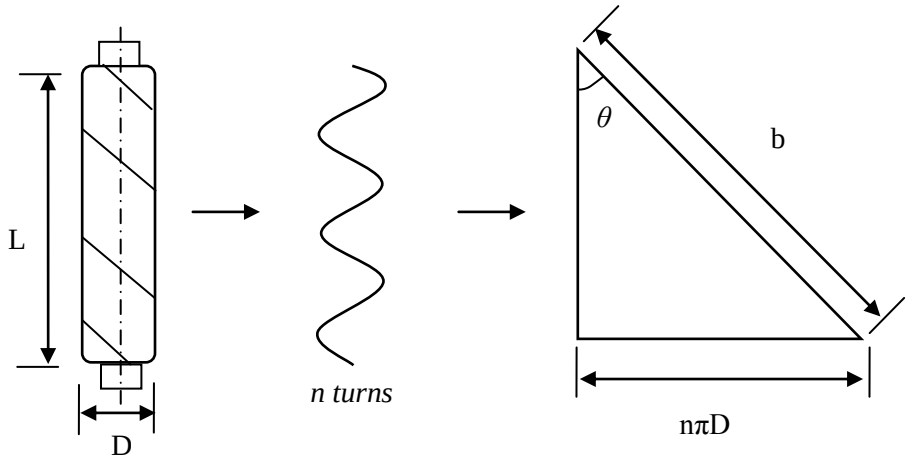

Figure 4-2 : The geometry of McKibben [71].

From Figure 4-2, we could express the L and D as next equations:

$$L = b\ \cos\theta \qquad 4\text{-}4$$

$$D = \frac{b\ \sin\theta}{\pi n} \qquad 4\text{-}5$$

The volume of a cylinder is:

$$V = \frac{\pi D^2 L}{4} = \frac{b^3}{4\pi n^2}\sin^2\theta\cos\theta \qquad 4\text{-}6$$

From these equations, the axial force could be expressed:

$$F = -P'\frac{dV}{dL} = -P'\frac{dV/d\theta}{dL/d\theta} \qquad 4\text{-}7a$$

$$F = \frac{\pi D_{\theta=90}^2 P'}{4}(3\cos^2\theta - 1) \qquad 4\text{-}7b$$

Where $D_{\theta=90}$ is the diameter when$\theta = 90^o$, $D_0 = \frac{b}{\pi n}$. Due to the difficulty of measuring of fibre angle ±θ, it is worth expressing the equation in terms of tube length L, and uncoiled length of fib$re\ b$, substituting (4-4) and (4-5) into (4-7) and rearranging the equation:

$$F = P'\left(\frac{3L^2 - b^2}{4\pi n^2}\right) \qquad 4\text{-}8$$

The equation illustrates that there are three variable parameters of this device: an applied force, internal pressure, and the length of the tube. The effective hydraulic area of the actuator will be:

$$A = \left(\frac{3L^2 - b^2}{4\pi n^2}\right) \qquad 4\text{-}9$$

4-4 Validation of the Model

This section explains the experimental procedures to determine the effective hydraulic area, and the experimental validation of the static model of the test rig. The tools and materials used in this experiment are: McKibben actuator, rubber tube, ball valve and frame. The test rig has been installed as shown in Figure 4-1; the overall inputs to the test rig are presented in table 4-1.

Table 4-1: the input parameter of the test rig

Input	**Value**
Length	$L = 0.212\ m$
Diameter	$D = 0.011m$
Length of uncoiled fibre	$b = 0.2337\ m$
Number of turns	$n = 2.847$

Determining the effective hydraulic area experimentally will be achieved by using an isometric test (The length of McKibben tube is a constant during the procedures of experiment). The procedures of experiment are starting by filling water inside McKibben tube then ball valve will be closed. The force will be applied to the system from 0 to maximum 140 N. Because the McKibben tube is filled with water, and water is incompressibility fluid, the length of the tube will not change. The pressure will recorded at each applied force by using the digital gage pressure. Three different initial lengths (21.5cm, 17.2cm, and 12cm) have been tested in the experiments, the results are shown in table 4-2.

Table 4-2: The result of isometric test

Force (N)	Pressure (N/m^2)		
	Initial length 21.5 cm	Initial length 17.2 cm	Initial length 12 cm
0	0	0	0
20	25000	24500	23000
40	49000	48500	46500
60	76000	76700	74500
80	104000	103300	99000
100	131000	130000	127000
120	159000	157000	155000
140	186000	184000	182000

Figure 4-3 shows force-pressure relationship at different lengths. The effective hydraulic area is equal to the inverse of gradient of the line which equals 0.000769 m^2. Numerically, the effective hydraulic area is also determined by using equation 4-9 which is equal to0.000788 m^2.

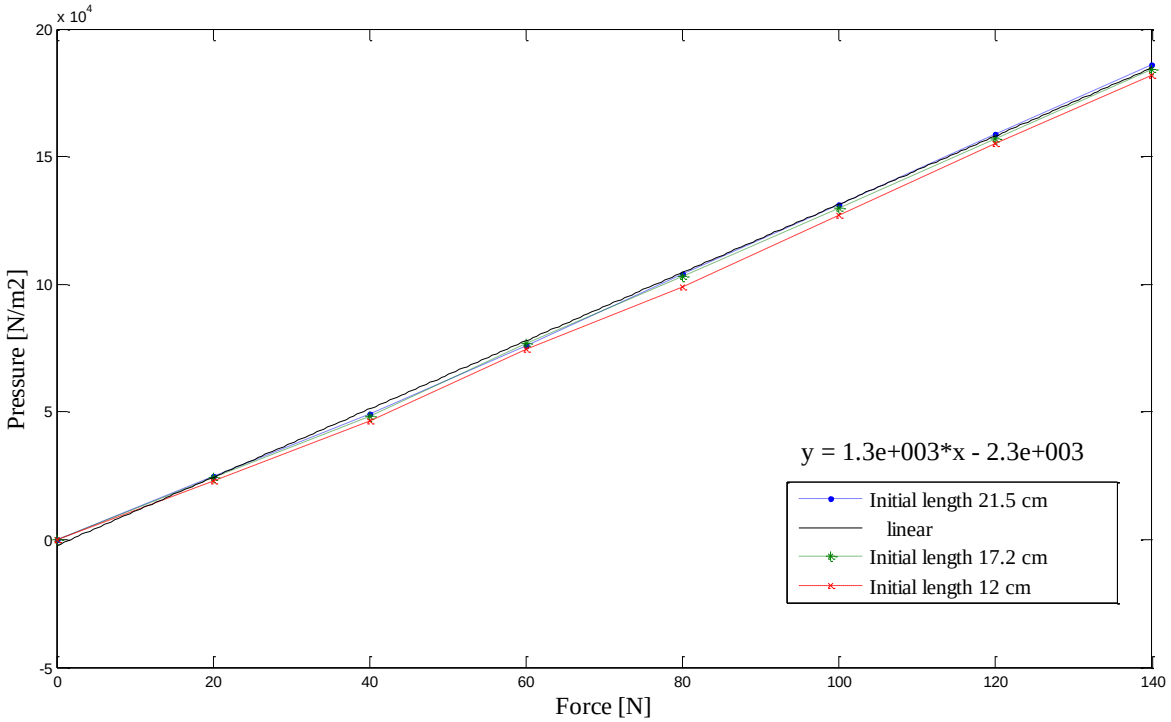

Figure 4-3: The relationship between force and pressure for McKibben tube at constant length.

Validation of the model equation (equation 4-8) could be achieved by using the isobaric test. In this test, the internal pressure is constant in the McKibben tube and the other parameters (force and length) will be changed. Because it is not easy to ensure pressure is constant during a changing load, the isotonic test (constant applied force and changing pressure and length of McKibben tube) will be carried out in this report. The procedures of the test are: The actuator was loaded to known load (25 N), and then internal pressure was increased 0.5 bar increments to a maximum of 4 bar. The internal pressure P, length of McKibben tube L and applied load F are all recorded during each step of the test. Three separate tests were run, each with a different load (25N, 50N and 75 N). Figure 4-4 is a plot of the pressure-length relationship at different loads. The force-length relationship at each pressure could be plotted by using an isobaric test.

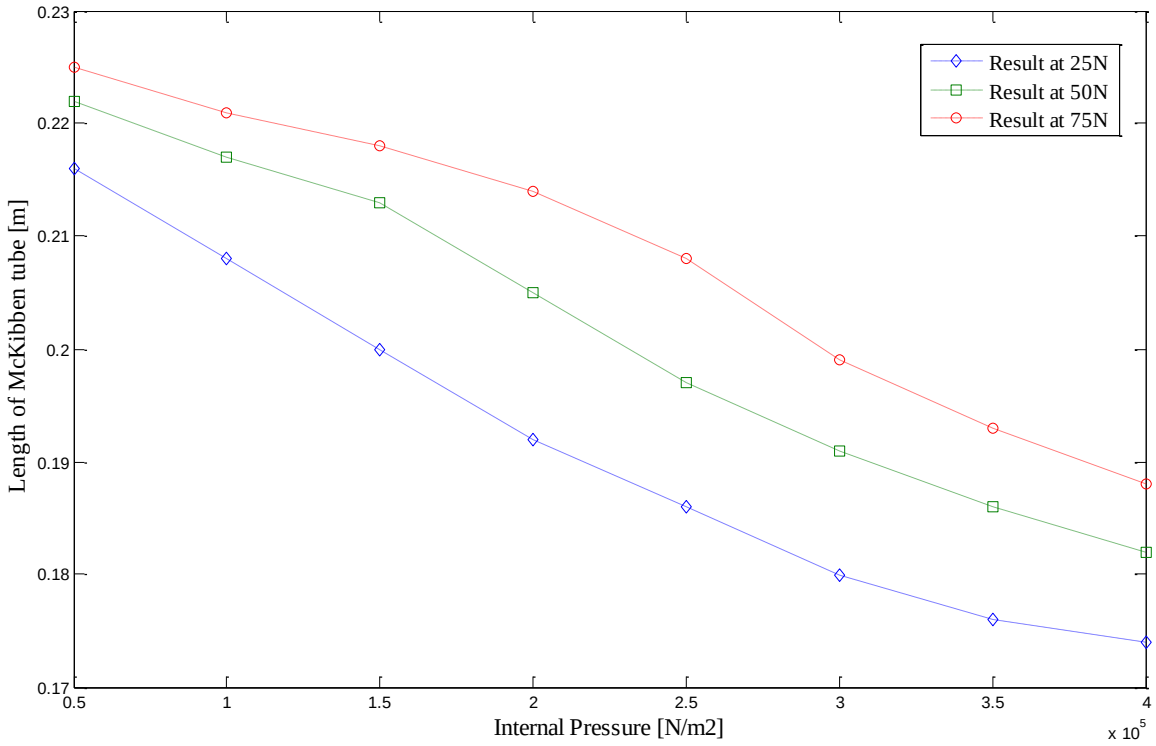

Figure 4-4: The relationship between length and pressure for McKibben tube at constant load.

The experimental results were compared with modelling results; the length of the McKibben tube is calculated by rearranging equations 4-8 as shown in equation 4-10:

$$L = \sqrt{\left[F + \frac{P'b^2}{4\pi n^2}\right]\left[\frac{4\pi n^2}{3P'}\right]} \qquad 4\text{-}10$$

The Matlab code that was used to plot this equation and the entire results which were achieved by modelling and experiments are shown in Appendix B. Figure 4-5 shows the experimental results which are compared with the modelling results at a constant load 25 N.

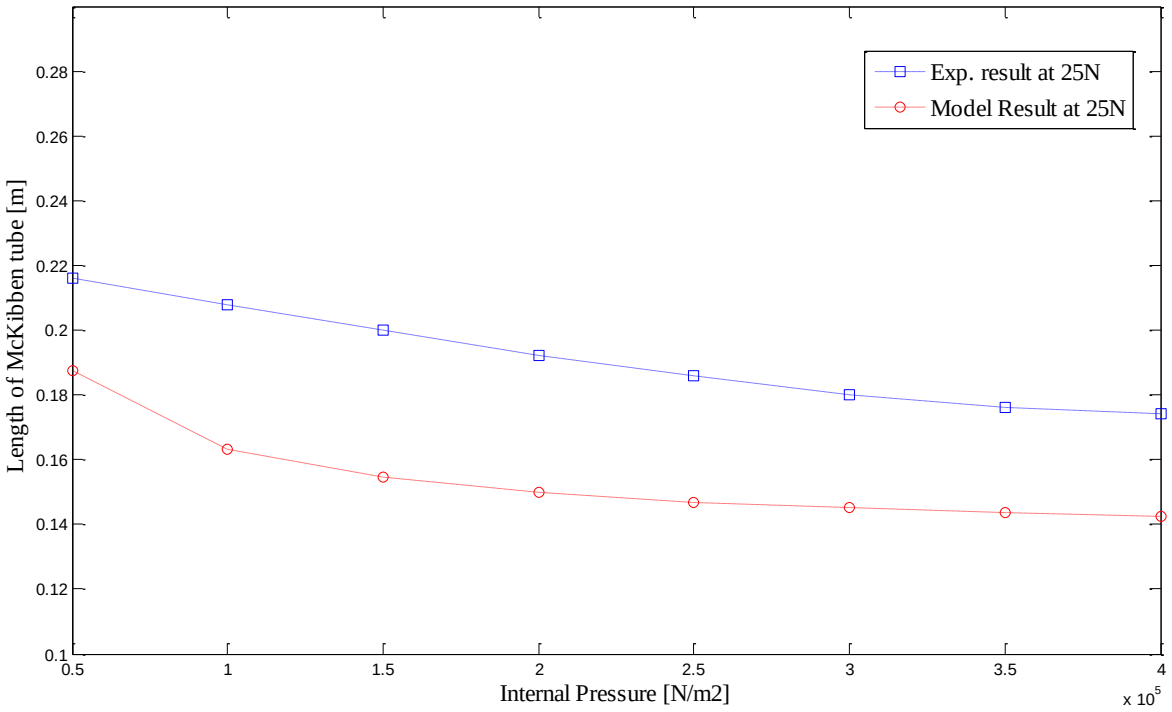

Figure 4-5: Plot of model and experimental result between length and internal pressure for McKibben actuator at load 25N.

The figure shows differences between the modelling results and experimental results, and the accuracy of the model is about 80%. These errors occurred due to ignoring some parameters, such as: neglecting the strain energy of the rubber tube, and ignoring force losses in the system due to friction between fibres and friction between the inner tube and outer tube. Moreover, the McKibben actuator is considered as an ideal cylindrical shape. To minimize these differences, it is important to consider these factors.

4-5 Improved Static Model of McKibben Actuator

The accuracy of the previous model of the McKibben tube is about 80 %. An improved model which could provide a higher accuracy is attempted in this section. To improve the model of McKibben behaviour, the model is extended by introducing an elastic energy of inner tube:

$$dW_{in} = dW_{out} + V_r dW \qquad 4\text{-}13$$

Where V_r the volume is occupied by the inner tube, and W is the strain energy density function. From the previous analysis of input work and output work:

$$P'dV = -FdL + V_r dW \quad \text{4-14a}$$

Or

$$F = -P'\frac{dV}{dL} + V_r\frac{dW}{dL} \quad \text{4-14b}$$

To determine the strain energy density of the inner tube, the Mooney-Rivlin model was used in some previous works [79, 80] and the Neo-Hookean model in another [85]. For simplicity, the rubber tube will be assumed to behave as a Neo–Hookean solid. The strain energy function of the actuator W could be expressed as a function of the first invariant of strain [86].

$$W = \frac{\mu_r}{2}[I_1 - 3] \quad \text{4-15}$$

μ_r is the shear modulus for infinitesimal deformations [86], and I_1 strain invariants which could be expressed:

$$I_1 = \lambda_1^2 + \lambda_2^2 + \lambda_3^2 \quad \text{4-16}$$

$\lambda_i (i = 1,2,3)$ are the principle stretches. $\lambda_1 = \frac{L}{L_0}$, $\lambda_2 = \frac{D}{D_0}$ and $\lambda_3 = \frac{1}{\lambda_1\lambda_2}$.

Where L and D are instantaneous length and diameter, while L_0 and D_0 are initial length and diameter of the tube, respectively. So, W can be expressed as next the equation:

$$W = \frac{\mu_r}{2}[\lambda_1^2 + \lambda_2^2 + \lambda_3^2 - 3] \quad \text{4-17a}$$

or

$$W = \frac{\mu_r}{2}\left[\left(\frac{L}{L_0}\right)^2 + \left(\frac{D}{D_0}\right)^2 + \left(\frac{D_0 L_0}{DL}\right)^2 - 3\right] \quad \text{4-17b}$$

From the geometry model in Figure 4-2, the diameter of the tube could be expressed in terms of length of tube:

$$D^2 = \frac{b^2 - L^2}{\pi^2 n^2} \quad \text{4-18}$$

Therefore strain energy density of inner tube W is determined by using the next equation:

$$W = \frac{\mu_r}{2}\left[\frac{L^2}{L_0^2} + \frac{b^2 - L^2}{D_0^2\pi^2 n^2} + \frac{D_0^2 L_0^2 \pi^2 n^2}{L^2(b^2 - L^2)} - 3\right] \quad \text{4-19}$$

The derivative strain energy density regarding the length:

$$\frac{dW}{dL} = \frac{\mu_r}{2}\left[\frac{2L}{L_0^2} + \frac{-2L}{D_0^2\pi^2 n^2} + \frac{-2D_0^2 L_0^2 \pi^2 n^2 (b^2 - 2L^2)}{L^3(b^2 - L^2)^2}\right] \quad \text{4-20}$$

Therefore, the force output of the actuator could be expressed:

$$F = P'\left(\frac{3L^2-b^2}{4\pi n^2}\right) + \frac{V_r \mu_r}{2}\left[\frac{2L}{L_0^2} + \frac{-2L}{D_0^2\pi^2 n^2} + \frac{-2D_0^2 L_0^2 \pi^2 n^2 (b^2-2L^2)}{L^3(b^2-L^2)^2}\right] \quad 4\text{-}21$$

4-6 The Results and Discussion

The basic model has been investigated by using isotonic tests; also the improved model will be validated by using the same techniques and the tools and materials used in this experiment were similar to the previous experiment. The test rig is shown in Figure 4-1; the new experimental parameter in this model is shown in Table 4-3:

Table 4-3: the input parameter of the test rig

Input	Value
Shear modulus of rubber [87].	$\mu_r = 0.0006$ GPa.
Thickness of inner tube	$t_o = 0.0003\ m$

The Matlab code is used to calculate the equation of the improved model (equation 4-21). The script of Matlab is shown in Appendix C. Figure 4-6 shows the experimental results which are compared with the modelling results at a constant load 25 N.

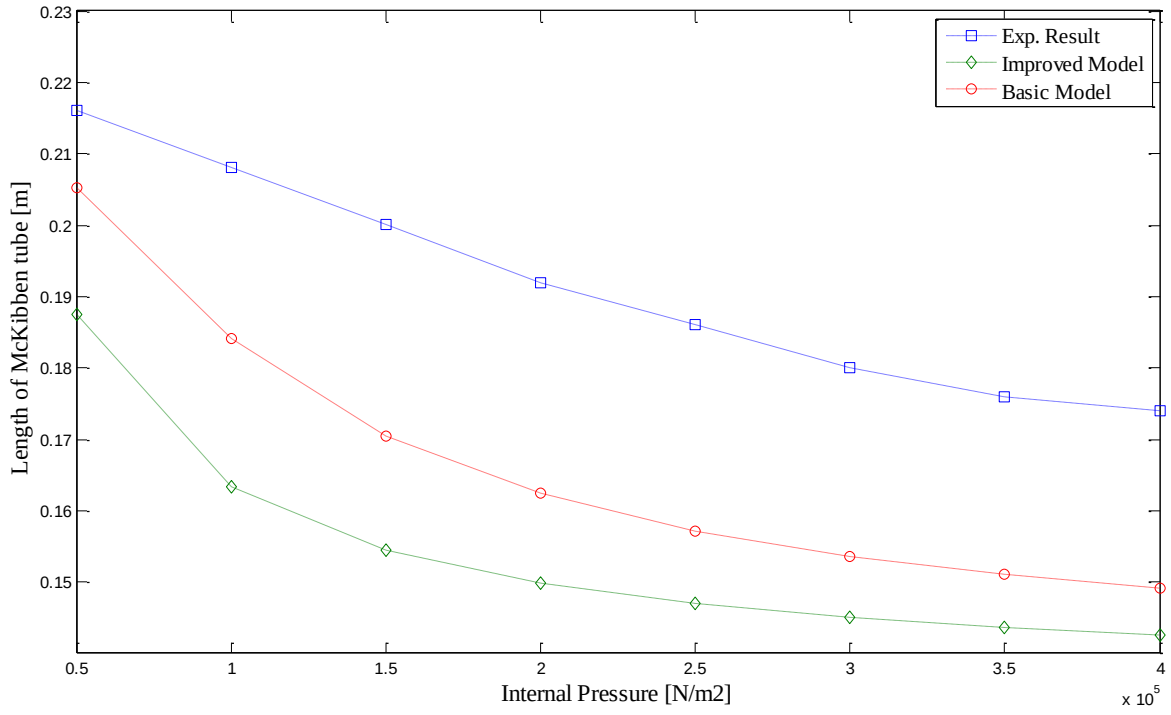

Figure 4-6: Plot of basic model, improved model and experimental result between length and internal pressure for McKibben actuator at load 25

The figure shows the improved model gives better results than the basic model. Although there are differences between the modelling results and experimental results, and solving the new model is more difficult, the accuracy of the model is above 85%. To minimize these differences, it is important to consider the following factors:

- The equation of the model was based on considering that the McKibben actuator has the ideal cylindrical shape. However, in reality the tube is not regular as it was assumed. Therefore, the accuracy of the model will be improved if we could find the derived dV/dL (in equation 4-3b) for a more realistic shape.
- There are force losses in the system due to friction between fibres and friction between the inner tube and outer tube, although the losses here are small, but it has an effect on the accuracy of the model.

This model is adequate and simple enough for dynamic simulation and control.

The model is shown to have less accuracy at low pressure, and the error is bigger when applying higher loads as shown in Figure 4-7. The final addition to the model is to capture the end effects, which changes in the output of the force at the length limits. When the actuator is reaching the maximum length $L_{\max}$ (length saturation), the stretching will be occurring in the fibres; therefore the force will be dependant on the material of the fibre. While the force is zero if the length of actuator is less than minimum length $L_{\min}$, this model is shown in next equations [78].

$$F = \begin{cases} \frac{P' b^2}{4\pi n}\left(\frac{3L^2}{b^2} - 1\right) + F_{max} & if\ (L > L_{\min}) \\ 0 & if\ (L < L_{\min}) \end{cases} \quad \text{4-22a}$$

Where:

$$F_{max} = \begin{cases} K_{\text{fiber}}(L - L_{max}) & if\ (L > L_{\max}) \\ 0 & if\ (L < L_{\max}) \end{cases} \quad \text{4-22b}$$

Where: b length of uncoiled fiber, n number of turns, K_{fiber} stiffness of fibre material.

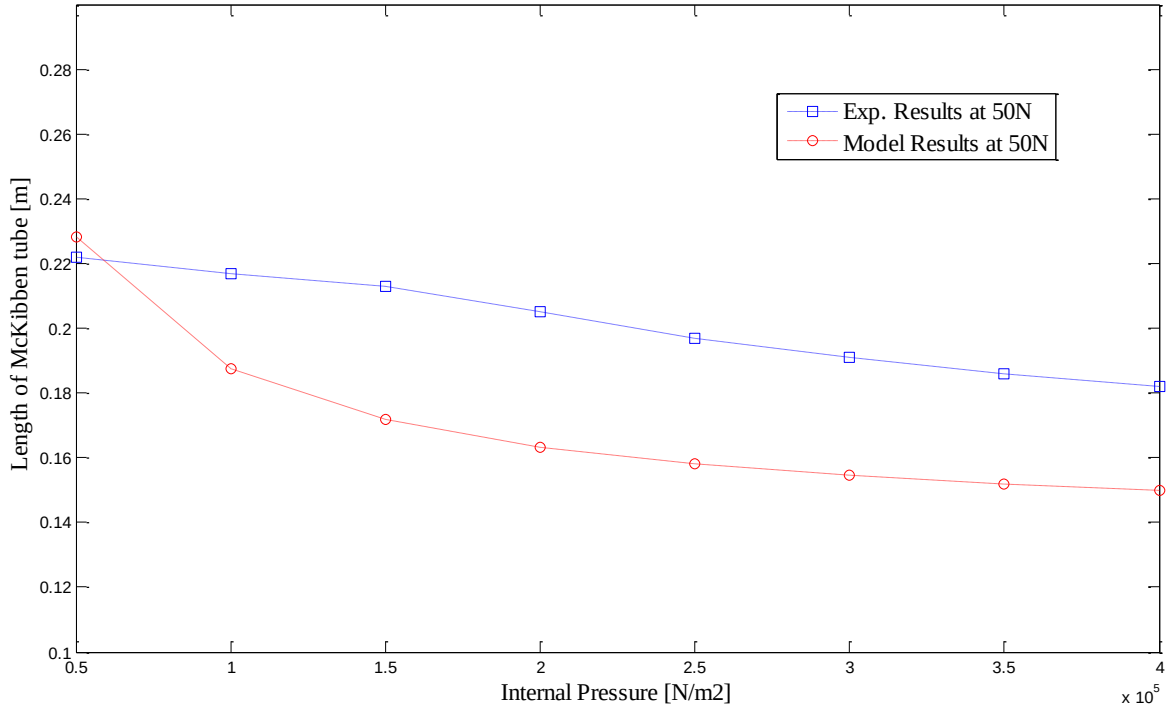

Figure 4-7: Plot of model and experimental result between length and internal pressure for McKibben actuator at load 50N.

CHAPTER FIVE: CONCLUSIONS AND FUTURE WORK

5-1 Conclusions

Smart fluid is considered as one of the most superior means of control of vibration, and there are many of semi-active applications which profit from the characteristics of smart fluid, which have been employed successfully. However, a conventional MR damper has dry sealing frictions which cause a vibration transmission to the equipment. To reduce the friction in a device, the possibility of using a McKibben actuator instead of a hydraulic actuator to design an MR damper is studied. The main conclusions from this study can be summarized as follows:

- The principles of smart fluids have been investigated; the previous applications and modelling are also reviewed.
- The concepts of a McKibben actuator and modelling approaches of a McKibben actuator have been introduced.
- A test rig of a McKibben actuator has been designed
- The effective hydraulic area of a McKibben actuator is theoretically determined, and the expression of the theoretically effective area was validating experimentally
- Simple and improved models of the test rig were modelled under static load. Then the model was validated experimentally.

The model predicts the behaviour of the test rig under static load. The model is simple and its accuracy is about 85%. Its accuracy could be improved by taking into account: the effect of the end tube and the friction factor between fibres.

5-2 Future Study

The main purpose of this research is to study the possibility of design a smart fluid damper by using McKibben actuator. This research is the first steps toward designing MR damper by using McKibben actuator. The following tasks should be carried out in further study:

First task: it is important to model and validate the behaviour of a McKibben actuator under dynamic load. In this case; the effect of a ball valve will be considered. It also requires installing a digital instrumentation system to record all variable parameter's values during

loading. The dynamic model of the test rig requires three equations of motion to capture the dynamic behaviour; the first equation of motion defines the vibration of suspended mass, and it is defined by using Newton's Second Law. The second equation represents the movement of the working fluid, and the flow continuity equation should be used. And the third equation captures the characteristics of pressurized air; the polytrophic law for the compression of gases is used to determine this equation.

Second task: magneto-rheological fluid will be used in the McKibben tube instead of water, and using a Magnetorheological MR Valve instead of a ball valve. This step requires designing an MR valve, then modelling the new system and validating the model. In this case the working fluid will be smart fluid, which will move in and out of the McKibben tube through a valve. By designing the MR valve and using it instead of the ordinary valve, the magnetic field could restrict the fluid inside the tube, while an absence of magnetic field would allow the fluid to flow out of the tube. The most important region of modelling an MR valve is the active region; this region is modelled by using a Bingham plastic flow between parallel flat plates. The model of a smart fluid device depends on the geometry of the valve, the geometry of the actuator, and the properties of the fluid. The variable of the actuator geometry is the effective hydraulic area. This area has been determined experimentally and theoretically, therefore it is important to find this variable to implement the model of smart fluid devices.

Third task: designing the control strategy of this damper. The literature review of the control strategy of a smart fluid damper is introduced in Chapter two, section 2-8. There are two objectives that must be addressed in order to design controllers for smart fluid based vibration systems: the first objective is to determine the desired damping force that will provide the optimal performance; the second objective is to calculate the input current that generates this force. Because of the nonlinear behaviour of smart fluid, different strategies have been used to track force, such as: on/off method, linear relationship between control of the current and the desired damping force, and linearization of the feedback of force/velocity behaviour of a smart fluid damper.

6-RERERENCES

1. Mead, D.J., *Passive vibration control*. 2000: John Wiley and Sons Ltd.
2. Wang, J., et al., *Active vibration control for lathe based neural network*. 2011. p. 183-187.
3. Daley, S., et al., *Active vibration control for marine applications.* Control Engineering Practice, 2004. 12(4): p. 465-474.
4. Karnopp, D., M.J. Crosby, and R.A. Harwood, *Vibration control using semi-active force generators*. Journal of Engineering for Industry, 1974. 96 (2): p. 619-626
5. Schwartz, M., ed. *Vibration Control for Smart Structures*. Smart Materials. 2009, Taylor & Francis Group.
6. Hall, K.L., *Dynamic Control For a Pneumatic Muscle Actuator to Achieve Isokinetic Muscle Strengthening* 2011, Wright State University.
7. Scarborough, L.H., C.D. Rahn, and E.C. Smith, *Fluidic composite tunable vibration isolators.* Journal of Vibration and Acoustics, Transactions of the ASME, 2012. 134(1).
8. Spencer, B.F. and S. Nagarajaiah, *State of the Art of Structural Control.* Journal of Structural Engineering, 2003. 129(7): p. 12.
9. Sims, N., R. Stanway, and A. Johnson, *Vibration control using smart fluids: A state-of-the-art Review.* The Shock and Vibration Digest, 1999. 31(3): p. 195-203.
10. Jolly, M.R., J.W. Bender, and J.D. Carlson, *Properties and Applications of Commercial Magnetorheological Fluids.* Journal of Intelligent Material Systems and Structures, 1999. 10(1): p. 5-13.
11. Wang, D.H. and W.H. Liao, *Magnetorheological fluid dampers: a review of parametric modelling.* SMART MATERIALS AND STRUCTURES, 2011.
12. Yang, G., et al., *Large-scale MR fluid dampers: Modeling and dynamic performance considerations.* Engineering Structures, 2002. 24(3): p. 309-323.
13. Seong, M.-S., S.-B. Choi, and C.-H. Kim, *Design and Performance Evaluation of MR Damper for Integrated Isolation Mount.* Journal of Intelligent Material Systems and Structures, 2011. 22(15): p. 1729-1738.
14. Karnopp, D., *Computer Simulation of Stick-slip Friction in Mechanical Systems.* Journal of Dynamic Systems, Measurement and Control, Transactions of the ASME, 1985. 107(1): p. 100-103.
15. Tuijthof, G.J.M. and J.L. Herder, *Design, actuation and control of an anthropomorphic robot arm.* Mechanism and Machine Theory, 2000. 35(7): p. 945-962.
16. Koeneman, E.J., et al. *A pneumatic muscle hand therapy device*. in *Engineering in Medicine and Biology Society, 2004. IEMBS '04. 26th Annual International Conference of the IEEE*. 2004.
17. Caldwell, D.G., et al., *A pneumatic muscle actuator driven manipulator for nuclear waste retrieval.* Control Engineering Practice, 2001. 9(1): p. 23-36.
18. Kenneth, K.K.K. and R. Bradbeer, *Static Model of the Shadow Muscle under Pneumatic Testing.* Department of Electronic Engineering, City University of Hong Kong, Kowloon, Hong Kong, 2006.
19. Shan., Y., et al., *Variable Stiffness Structures Utilizing Fluidic Flexible Matrix Composites.* Journal of intelligent material system and structures 2009. 20: p. 443.
20. Lightner, S., *The Fluidic Muscle: A 'New' Development.* The International Journal of Modern Engineering, 2002. 2.
21. Winslow, W.M., *Method and means for translating electrical impulses into mechanical forces.* Paten No. 2471850., 1947.
22. Stanway, R., J.L. Sproston, and A.K. El-Wahed, *Applications of electro-rheological fluids in vibration control: A survey.* Smart Materials and Structures, 1996. 5(4): p. 464-482.
23. Carlson, J.D., D.M. Catanzarite, and K.A. St. Clair, *Commercial Magnet-rheological Fluid Devices.* International Journal of Modern Physics B, 1996. 10(23n24): p. 2857-2865.
24. Batterbee, D.C., *Magnetorheological shock absorbers: Modelling, Design, and control* in *Department of Mechanical engineering*. 2006, PhD thesis, University of Sheffield: Sheffield.

25. Wang, et al., *Study of field-controllable, electro- and magneto-rheological fluid dampers in flow mode using Herschel-Bulkley theory.* Smart Structures and Materials 2000.
26. Wereley, N.M., et al., *Magnetorheological dampers in shear mode.* Smart Materials and Structures 2008. 17 (1).
27. Giorgetti, A., et al., *Design and testing of a MRF rotational damper for vehicle applications.* Smart Materials and Structures, 2010. 19(6): p. 065006.
28. Sukhwani, V.K. and H. Hirani, *Design, development, and performance evaluation of high-speed magnetorheological brakes.* Proceedings of the Institution of Mechanical Engineers, Part L: Journal of Materials Design and Applications, 2008. 222(1): p. 73-82.
29. Stanway, R., et al., *ER fluids in the squeeze-flow mode: an application to vibration isolation.* Journal of Electrostatics, 1992. 28(1): p. 89-94.
30. Stanway, R., et al., *ER Fluids in the Squeeze-Flow Mode: An Application to Vibration Isolation, Journal of Electrostatics.* Journal of Electrostatics, 1992. Vol. 28, No. 1, 1992.
31. Sproston, J.L., A.K. El Wahed, and R. Stanway. *Electrorheological fluids in dynamic squeeze flow*. in *Conduction and Breakdown in Dielectric Liquids, 1996, ICDL '96., 12th International Conference on*. 1996.
32. Wereleyy, N.M. and L. Pang, *Nondimensional analysis of semi-active electrorheological and magnetorheological dampers using approximate parallel plate models.* SMART MATERIALS AND STRUCTURES, 1998. 7: p. 732-743.
33. Kamath G M, Hurt M K, and W.N. M., *Analysis and testing of Bingham plastic behavior in semi-active electrorheological fluid dampers.* SMART MATERIALS AND STRUCTURES, 1996. 5: p. 576-590.
34. Kulkarni, P., et al., *Study of the Behavior of MR Fluids in Squeeze, Torsional and Valve Modes.* Journal of Intelligent Material Systems and Structures, 2003. 14(2): p. 99-104.
35. Ashfak, A., et al., *Design, Fabrication and Evaluation of MR Damper.* International Journal of Aerospace and Mechanical Engineering 5:1, 2011.
36. Lee, H.-S. and S.-B. Choi, *Control and Response Characteristics of a Magneto-Rheological Fluid Damper for Passenger Vehicles.* Journal of Intelligent Material Systems and Structures, 2000. 11(1): p. 80-87.
37. Simon, D.E., *Experimental Evaluation of Semiactive Magnetorheological Primary Suspensions for Heavy Truck Applications*, in *Virginia Polytechnic Institute and State University*. 1998.
38. Stanway, R., J.L. Sproston, and A.K. El-Wahed, *Applications of electro-rheological fluids in vibration control: a survey.* SMART MATERIALS AND STRUCTURES, 1996. 5.
39. Hong, S.-R. and S.-B. Choi, *Vibration Control of a Structural System Using Magneto-Rheological Fluid Mount.* Journal of Intelligent Material Systems and Structures, 2005. 16(11-12): p. 931-936.
40. Mehmet, A., *Personal Communication.* 2013.
41. Spencer, B.F.J.D., S J . Sain, M K . Carlson, J D., *Phenomenological model for magnetorheological dampers.* J. Eng. Mech. ASCE 123 230–8, 1997.
42. Phillips, R.W., *Engineering applications of fluids with a variable yield streess*, in *Department of Mechanical Engineering.* 1969, University of California at Berkeley.
43. Wang, et al., *Study of field-controllable, electro- and magneto-rheological fluid dampers in flow mode using Herschel-Bulkley theory.* Smart Structures and Materials, 2000.
44. Gamota, D. and F. Filisko, *Dynamic mechanical studies of electrorheological materials: moderate frequencies.* J. Rheol, 1991.
45. Stanway, R.S., J L . EL-Wahed, A K., *Non-linear modelling of an electro-rheological vibration damper.* Journal of Electrostatics, 1987. 20.
46. Kamath, G.M., N.M. Wereley, and M.R. Jolly, *Characterization of magnetorheological helicopter lag dampers.* J. Am. Helicopter Soc. 44 234–48, 1999.
47. Pang, L., G.M. Kamath, and N.M. Wereley, *Analysis and Testing of Linear Stroke Magnetorheological Damper.* The AIAA/ASME/AHS Adaptive Structures Forum, 1998. Vol. CP9803,: p. 2841-2856.

48. Zhou, Q., S.R.K. Nielsen, and W.L. Qu, *Semi-active control of three-dimensional vibrations of an inclined sag cable with magnetorheological dampers.* Journal of Sound and Vibration, 2006. 296(1-2): p. 1-22.
49. Kwok, N.M., et al., *A novel hysteretic model for magnetorheological fluid dampers and parameter identification using particle swarm optimization.* Sensors and Actuators A: Physical, 2006. 132(2): p. 441-451.
50. Sims, N.D., N.J. Holmes, and R. Stanway, *A unified modelling and model updating procedure for electrorheological and magnetorheological vibration dampers.* SMART MATERIALS AND STRUCTURES, 2004. 13: p. 100-121.
51. Wang, D.H. and W.H. Liao, *Semiactive Controllers for Magnetorheological Fluid Dampers.* Journal of Intelligent Material Systems and Structures, 2005. 16(11-12): p. 983-993.
52. Guo, D.L., H.Y. Hu, and J.Q. Yi, *Neural Network Control for a Semi-Active Vehicle Suspension with a Magnetorheological Damper.* JVC/Journal of Vibration and Control, 2004. 10(3): p. 461-471.
53. Atray, V.S. and P.N. Roschke, *Neuro-fuzzy control of railcar vibrations using semiactive dampers.* Computer-Aided Civil and Infrastructure Engineering, 2004. 19(2): p. 81-92.
54. Yoshida, O. and S.J. Dyke, *Seismic Control of a Nonlinear Benchmark Building Using Smart Dampers.* Journal of Engineering Mechanics, 2004. 130(4).
55. Simon, D. and M. Ahmadian, *Vehicle evaluation of the performance of the magnetorhological dampers for heavy truck suspension.* Journal of Vibration and Acoustics, 2001.
56. Sims, N.D., et al., *Controllable viscous damping: an experimental study of an electrorheological long-stroke damper under proportional feedback control.* SMART MATERIALS AND STRUCTURES, 1999. 8(5): p. 601-615.
57. Shan, Y., et al., *Nonlinear-elastic finite axisymmetric deformation of flexible matrix composite membranes under internal pressure and axial force.* Composites Science and Technology, 2006. 66(15): p. 3053-3063.
58. Kyung, K., et al. *Characteristics of the muscle activities for the elderly wearing the lower limb orthosis during gait on the treadmill*. in *ICCAS-SICE, 2009*. 2009.
59. Caldwell, D.G., et al., *"Soft" exoskeletons for upper and lower body rehabilitation - Design, control and testing.* International Journal of Humanoid Robotics, 2007. 4(3): p. 549-573.
60. Chen, Y., et al., *Structural design and analysis of morphing skin embedded with pneumatic muscle fibers.* Smart Materials and Structures, 2011. 20(8): p. 085033.
61. Davis, S. and D.G. Caldwell, *Braid Effects on Contractile Range and Friction Modeling in Pneumatic Muscle Actuators.* The International Journal of Robotics Research, 2006. 25(4): p. 359-369.
62. website, F.C., *Fluidic muscle/ http://www.festo.com/cms/en_corp/9790.htm*.
63. Dongseok, R., et al. *Micro hydraulic system using slim artificial muscles for a wearable haptic glove*. in *Intelligent Robots and Systems, 2008. IROS 2008. IEEE/RSJ International Conference on*. 2008.
64. Li, S., et al., *A variable transverse stiffness sandwich structure using fluidic flexible matrix composite (F2MC).* Active and Passive Smart Structures and Integrated Systems 2008; San Diego, 2008.
65. Philen, M., *On the applicability of fluidic flexible matrix composite variable impedance materials for prosthetic and orthotic devices.* Smart Materials and Structures, 2009.
66. Lotfi-Gaskarimahalle, A., et al. *Fluidic composite tuned vibration absorbers*. 2009.
67. Philen, M. *Semi-active vibration isolation using fluidic flexible matrix composite mounts*. 2009.
68. Focchi, M., et al. *Water/air performance analysis of a fluidic muscle*. in *Intelligent Robots and Systems (IROS), 2010 IEEE/RSJ International Conference on*. 2010.
69. Tondu, B., et al., *A pH-activated artificial muscle using the McKibben-type braided structure.* Sensors and Actuators A: Physical, 2009. 150(1): p. 124-130.
70. Yokota, S., et al., *Electro-conjugate fluid jet-driven micro artificial antagonistic muscle actuators and their integration.* Advanced Robotics, 2010. 24(14): p. 1929-1943.

71. Ching-Ping, C. and B. Hannaford. *Static and dynamic characteristics of McKibben pneumatic artificial muscles*. in *Robotics and Automation, 1994. Proceedings., 1994 IEEE International Conference on*. 1994.
72. Caldwell, D.G., G.A. Medrano-Cerda, and M. Goodwin, *Control of pneumatic muscle actuators.* Control Systems, IEEE, 1995. 15(1): p. 40-48.
73. Tsagarakis, N. and D.G. Caldwell. *Improved modelling and assessment of pneumatic muscle actuators*. in *Robotics and Automation, 2000. Proceedings. ICRA '00. IEEE International Conference on*. 2000.
74. Zhang, Z. and M. Philen, *Pressurized artificial muscles.* Journal of Intelligent Material Systems and Structures, 2012. 23(3): p. 255-268.
75. Doumit, M., A. Fahim, and M. Munro, *Analytical Modeling and Experimental Validation of the Braided Pneumatic Muscle.* Robotics, IEEE Transactions on, 2009. 25(6): p. 1282-1291.
76. Ching-Ping, C. and B. Hannaford, *Measurement and modeling of McKibben pneumatic artificial muscles.* Robotics and Automation, IEEE Transactions on, 1996. 12(1): p. 90-102.
77. Tondu, B. and P. Lopez, *Modeling and control of McKibben artificial muscle robot actuators.* Control Systems, IEEE, 2000. 20(2): p. 15-38.
78. Colbrunn, R.W., G.M. Nelson, and R.D. Quinn. *Modeling of braided pneumatic actuators for robotic control*. in *Intelligent Robots and Systems, 2001. Proceedings. 2001 IEEE/RSJ International Conference on*. 2001.
79. Klute, G.K. and B. Hannaford, *Accounting for Elastic Energy Storage in McKibben Atrificial Muscle Actuators.* Journal of Dynamic Systems, Measurement, and Control, 2000. 122(2): p. 386–388.
80. Sugimoto, Y., K. Naniwa, and K. Osuka. *Static and dynamic characteristics of McKibben pneumatic actuator for realization of stable robot motions*. in *Intelligent Robots and Systems (IROS), 2011 IEEE/RSJ International Conference on*. 2011.
81. Liu, W. and C.R. Rahn, *Fiber-Reinforced Membrane Models of McKibben Actuators.* Journal of Applied Mechanics, 2003. 70(6): p. 853-859.
82. Reynolds, D., et al., *Modeling the dynamic characteristics of pneumatic muscle.* 2003.
83. Zhu, X., X. Jing, and L. Cheng, *Magnetorheological fluid dampers: A review on structure design and analysis.* Journal of Intelligent Material Systems and Structures, 2012. 23(8): p. 839-873.
84. Lotfi-Gaskarimahalle, A., Scarborough III, L.H., Rahn, C.D. , Smith, E., *Fluidic composite tuned vibration absorbers.* ASME Conference on Smart Materials, Adaptive Structures and Intelligent Systems, 2009.
85. Trivedi, D., A. Lotfi, and C.D. Rahn, *Geometrically Exact Models for Soft Robotic Manipulators.* Robotics, IEEE Transactions on, 2008. 24(4): p. 773-780.
86. Chou-Wang, M.S. and C.O. Horgan, *Cavitation in nonlinear elastodynamics for neo-Hookean materials.* International Journal of Engineering Science, 1989. 27(8): p. 967-973.
87. Spanos, P., *Cure system effect on low temperature dynamic shear modulus of natural rubber.* Rubber World., 2003.

APPENDIX A: Analysis 2DOF System

- Matlab Simulink of 2DOF system

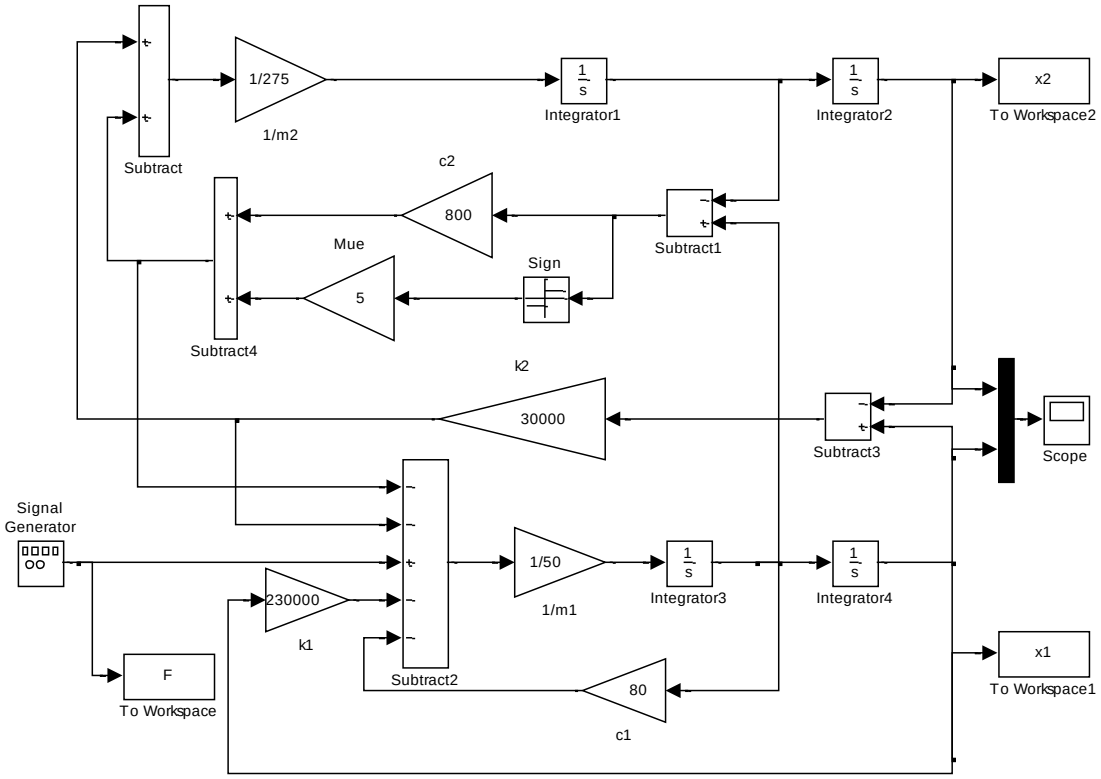

Figure A-1: Simulink model and value parameters of second degree of freedom

- Matlab Code for FRF

```
clear all
Fo=30;
Fs=1/5000;                      %fixed step size
ff=Fs;
cc=10;                          %number of cycle
wr=.1:0.1:16;                   %frequency of system rad/sn
for n=1:length(wr);
    fr(n)=wr(n);                %excitation frequency Hz
    t=cc/fr(n);                 %stop time s
    nxx=1/(fr(n)*ff);           %number of sample for one cycle
    sim sunday                  %Change model name to the name of your model
    yy(n)=max(F(end-nxx:end));
    mxa(n)=max(x1(end-nxx:end));
    mna(n)=min(x1(end-nxx:end));
    xxa(n)=(mxa(n)-mna(n))/2;
    yyy(n)=max(x2(end-nxx:end));
end
yu=230000*xxa./(yy);
yuu=230000*yyy./(yy);
plot(fr,yu)
hold all
%plot(fr,yuu)
```

APPENDIX B: Damping Ratio

Damping ratio is a dimensionless measure describing how oscillations in a system decay after a disturbance. If the single degree of freedom system (spring-mass-damper) is oscillated from its static position, the equation of motion is expressed as:

$$m\ddot{x} + c\dot{x} + kx = 0 \quad \text{B-1}$$

The characteristic equation of the system is:

$$ms^2 + cs + k = 0 \quad \text{B-2}$$

The roots of this equation are:

$$s_{1,2} = \frac{-c \mp \sqrt{c^2 - 4mk}}{2m} \quad \text{B-3}$$

Roots of the characteristic equation could be real and varied, or real and equal or complex number. It is depending on a radical value ($c^2 - 4mk$). The Critical damping c_c is the value of damping that gives two real and equal roots. In other words, critical damping is that becomes the radical value to zero. Therefore, the critical damping could be found as:

$$c_c^2 - 4mk = 0 \quad \text{B-4}$$

$$c_c = 2\sqrt{mk} \quad \text{B-5}$$

$$c_c = 2m\omega_n \quad \text{B-6}$$

Other values of damping is defined as a fraction of critical damping, it called damping ratio ζ:

$$\zeta = \frac{c}{c_c} \quad \text{B-7}$$

Therefore, the root of the characteristic equation can be re-written in term of damping ratio (ζ) as:

$$s_{1,2} = \left(\zeta \pm \sqrt{\zeta^2 - 1}\right)\omega_n \quad \text{B-8}$$

From these equations, the behaviour of solution is depending on the value of damping, there are three different cases:

- Under damped response: the value $c^2 - 4mk < 0$ or $\zeta < 1$.

- Critical damped response: the value $c^2 - 4mk = 0$ or $\zeta = 1$.

- Over damped response: the value $c^2 - 4mk > 0$ or $\zeta > 1$.

Figure B-1 is shown these responses.

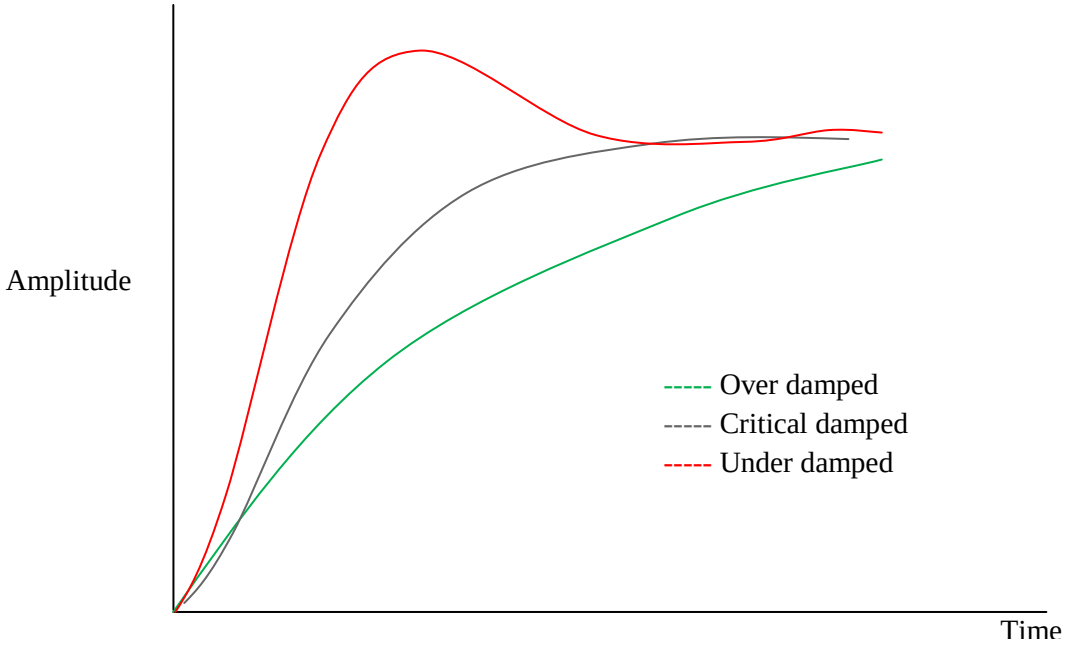

Figure B-1 Under damped, critical and over damped responses

APPENDIX C: Matlab Code for Simple Static Model

```
%Appendix C: Simple Static Model of McKibben tube
%Input
D0=0.011;                                   %diameter of tube
L0=0.212;                                   %Initial length of tube
b=0.2337;                                   %length of uncoiled fibre
n=sqrt((b^2-L0^2)/(D0^2*pi*pi));            %number of turns
pbar=0.5;                                   %pressure in bar unit
F=50                                        %force in Newton unit
while pbar<4                                %loop from 1 bar to 4 bar
      pbar=pbar+.5                          %increase 0.5 bar each step
      p=pbar*100000;                        %convert bar to N/m2
L=sqrt((F+(b^2*p/(4*pi*n^2)))*((4*pi*n^2)/(3*p))) %Equation 10
End
```

Table C-1 the experimental and modelling result of basic model.

Pressure bar	25 N			50 N			75 N		
	Exp. Result	Model Result	Error %	Exp. Result	Model Result	Error %	Exp. Result	Model Result	Error %
0.5	0.216	0.18755	13.170	0.222	0.22835	-2.86	0.225	0.26290	-16.84
1	0.208	0.16337	21.455	0.217	0.18755	13.57	0.221	0.20895	5.4514
1.5	0.2	0.15447	22.763	0.213	0.17181	19.337	0.218	0.18755	13.9669
2	0.192	0.14982	21.965	0.205	0.16337	20.306	0.214	0.17587	17.8139
2.5	0.186	0.14696	20.985	0.197	0.15809	19.749	0.208	0.16848	18.997
3	0.18	0.14503	19.427	0.191	0.15447	19.123	0.199	0.16337	17.903
3.5	0.176	0.14363	18.392	0.186	0.15183	18.368	0.193	0.15961	17.295
4	0.174	0.14257	18.062	0.182	0.14982	17.677	0.188	0.15674	16.624

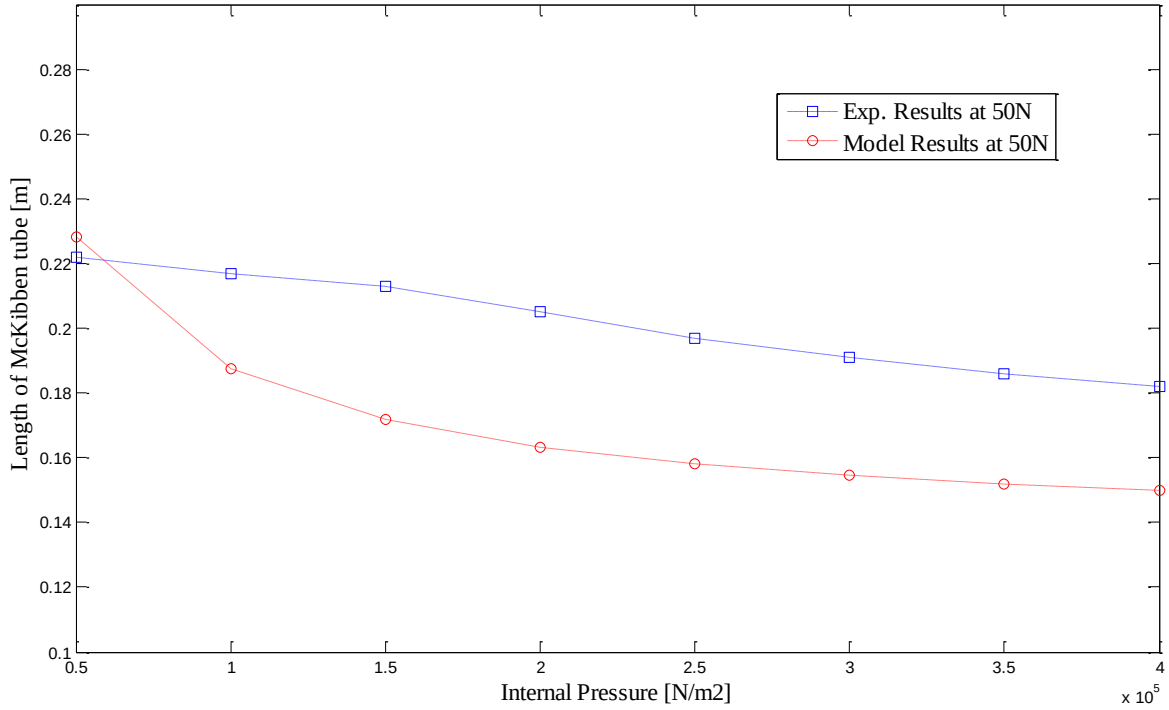

Figure C-1: Plot of Model and experimental result between length and internal pressure for McKibben actuator at load 50N.

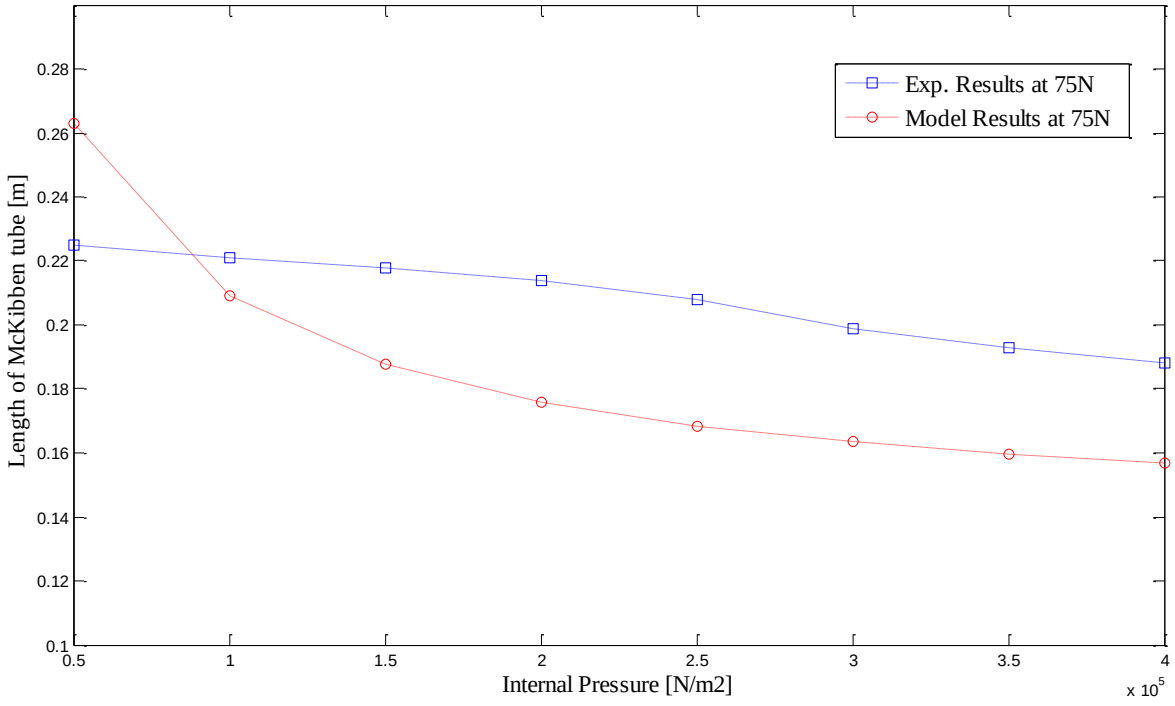

Figure C-2: Plot of Model and experimental result between length and internal pressure for McKibben actuator at load 75N

APPENDIX D: Matlab Code for Improved Static Model

```
%Appendix D: Improved Static Model of McKibben Tube
%Input
D0=0.011;                                % Initial diameter of tube
L0=0.212;                                %Initial length of tube
b=0.2337;                                %length of uncoiled fibre
n=sqrt((b^2-L0^2)/(D0^2*pi*pi));         %number of turns
t0=3e-4;                                 % thickness of inner tube (Bladder)
Er=1e7;                                  % inner tube (Bladder) stiffness
M=0.0006e9;                              %Shear modulus of inner tube
F=75                                     %force in Newton unit
pbar=0;                                  %pressure in bar unit
 while pbar<4                            %loop from 0.5 bar to 4 bar
   pbar=pbar+.5;                         %increase 0.5 bar each step
   p=100000*pbar;                        %convert bar to N/m^2
   a=-1;
   L=.26;                                % assuming L
while a<0
      L=L-.0001;
D=sqrt(b^2-L^2)/(n*pi);                 % Instance diameter of tube
Vr=t0*(L)*D*pi;                         %volume inner tube (Bladder)

%a=F-p*((3*L^2-b^2)/(4*pi*n^2));        % Equation 4-8
a=F-p*((3*L^2-b^2)/(4*pi*n^2))-(Vr*M/2*((2*L/L0^2)-(2*L/(D0^2*n^2*pi^2))-
(2*L0^2*D0^2*n^2*pi^2*(b^2-2*L^2)/(L^3*(b^2-L^2)^2)))); %Equation 4-21

end
x=L
end
```

Table D-1: The experimental and modelling result of improved model (isotonic test).

Pressure bar	25 N			50 N			75 N		
	Exp. Result	Model Result	Error %	Exp. Result	Model Result	Error %	Exp. Result	Model Result	Error %
0.5	0.216	0.2052	5	0.222	0.2153	3.01801	0.225	0.2599	-15.51
1	0.208	0.1842	11.442	0.217	0.2003	7.69585	0.221	0.2108	4.6153
1.5	0.2	0.1704	14.8	0.213	0.1852	13.0516	0.218	0.1973	9.4954
2	0.192	0.1624	15.416	0.205	0.1747	14.7804	0.214	0.1857	13.224
2.5	0.186	0.1572	15.483	0.197	0.1677	14.8731	0.208	0.1773	14.759
3	0.18	0.1536	14.666	0.191	0.1627	14.8167	0.199	0.1711	14.020
3.5	0.176	0.1511	14.147	0.186	0.159	14.5161	0.193	0.1664	13.782
4	0.174	0.1491	14.310	0.182	0.1561	14.2307	0.188	0.1628	13.404